Check for updates

Earth's Future

RESEARCH ARTICLE
10.1029/2022EF002972

Special Section:
CMIP6: Trends, Interactions, Evaluation, and Impacts

CMIP6 Earth System Models Project Greater Acceleration of Climate Zone Change Due To Stronger Warming Rates

Ali Serkan Bayar[1], M. Tuğrul Yılmaz[1], İsmail Yücel[1], and Paul Dirmeyer[2]

[1]Department of Civil Engineering, Water Resources Laboratory, Middle East Technical University, Ankara, Turkey, [2]Center for Ocean-Land-Atmosphere Studies, George Mason University, Fairfax, VA, USA

Abstract Warming climate and precipitation changes induce notable shifts in climate zones. In this study, the latest generation of global climate models from the Coupled Model Intercomparison Project Phase 6 (CMIP6) and the previous generation CMIP5 under high-emission scenarios are used together with observations and applied to the Köppen-Geiger climate classification. The aim is to shed light on how projected warming and changes in precipitation will influence future climate zones and their associated ecosystems while revealing differences between the two model generations. Compared to CMIP5 models, CMIP6 models exhibit slightly improved performance in replicating the observed Köppen-Geiger map for the historical (1976–2005) period and similar inter-model agreement for the future. The models show major changes in climate zones with a range of projections depending on which ensemble subset is used: 37.9%–48.1% of the global land area is projected to change climate zone by the end of the century, with the most pronounced changes expected over Europe (71.4%–88.6%) and North America (51.2%–65.8%). CMIP6 models project a higher rate of areal climate zone change (km^2/year) throughout the 21st century, which is mainly driven by their greater global land warming rates. Using a likely equilibrium climate sensitivity subset of CMIP6 models that is consistent with the latest evidence constrains the climate zone shifts, and their projections better match the results of CMIP5 simulations. Although the high warming rates of some CMIP6 models are less credible, the risks associated with them are greater, and they heighten the need for urgent action to preserve terrestrial ecosystems.

Plain Language Summary Köppen-Geiger climate classification is a tool to map regional climate zones based on a region's temperature and precipitation. In recent decades, increasing temperatures and changing precipitation trends have started to affect the distribution of those climate zones, and more extensive changes are expected throughout the 21st century. In this paper, we assess the observed and expected changes in the global distribution of Köppen-Geiger climate zones using observations along with the latest and the previous generation of global climate model projections. We find that shifts in climate zones are more pronounced in the latest generation of models due to their questionable greater global warming rate projections. Depending on which subset of model projections is used, up to half of the Earth's land area faces the risk of shifting to a different climate zone by the end of the century, with the greatest changes expected in Europe and North America. The rate of change (affected area per year) is also projected to accelerate through the 21st century, suggesting that vulnerable species and agricultural practices might have less time to adapt to changes in climate zones than previously projected.

Key Points:

- Coupled Model Intercomparison Project Phase 6 (CMIP6) exhibits slightly improved performance in simulating the globally observed historical Köppen-Geiger climate zones compared to CMIP5
- By the end of the century, 38%–48% of the global land area is projected to be in a different climate zone than today
- The rate of climate zone change is projected to accelerate, with more pronounced rates in CMIP6 due to considerably higher warming rates

Supporting Information:

Supporting Information may be found in the online version of this article.

Correspondence to:

A. S. Bayar and M. T. Yılmaz,
bayar.serkan@metu.edu.tr;
tuyilmaz@metu.edu.tr

Citation:

Bayar, A. S., Yılmaz, M. T., Yücel, İ., & Dirmeyer, P. (2023). CMIP6 Earth system models project greater acceleration of climate zone change due to stronger warming rates. *Earth's Future*, *11*, e2022EF002972. https://doi.org/10.1029/2022EF002972

Received 11 JUN 2022
Accepted 19 MAR 2023

Author Contributions:

Conceptualization: Ali Serkan Bayar
Data curation: Ali Serkan Bayar
Formal analysis: Ali Serkan Bayar

© 2023 The Authors. Earth's Future published by Wiley Periodicals LLC on behalf of American Geophysical Union. This is an open access article under the terms of the Creative Commons Attribution License, which permits use, distribution and reproduction in any medium, provided the original work is properly cited.

1. Introduction

Human activities are warming the planet at a pace that is unprecedented in the last two millennia (IPCC, 2021). The global mean temperature over land areas has increased to 1.59°C (90%–100% probability range: 1.34°C–1.83°C) above the pre-industrial period within the last decade (IPCC, 2021). Human influence can also be traced in precipitation trends over the globe (Kate & Céline, 2013; Zhang et al., 2007). Increasing temperatures and changing precipitation trends will severely threaten ecosystems and biodiversity (Leemans & Eickhout, 2004; Mccain & Colwell, 2011; Pereira et al., 2010; Williams et al., 2007). Changing climatic conditions are forcing species to move toward higher latitudes (I.-C. Chen et al., 2011; Parmesan & Yohe, 2003; Parmesan et al., 1999; Thomas & Lennon, 1999) and have possibly accelerated population extinctions (McLaughlin et al., 2002). Croplands are also shifting with the changes in the climate (Dirmeyer et al., 2014; King et al., 2018). Therefore, it is critical to quantify the observed and the projected climate change impacts on the Earth's terrestrial ecosystems (Cui et al., 2021).

Investigation: Ali Serkan Bayar, M. Tuğrul Yılmaz, İsmail Yücel, Paul Dirmeyer
Methodology: Ali Serkan Bayar, M. Tuğrul Yılmaz
Resources: M. Tuğrul Yılmaz
Software: Ali Serkan Bayar, M. Tuğrul Yılmaz
Supervision: M. Tuğrul Yılmaz
Visualization: Ali Serkan Bayar
Writing – original draft: Ali Serkan Bayar
Writing – review & editing: Ali Serkan Bayar, M. Tuğrul Yılmaz, İsmail Yücel, Paul Dirmeyer

Climate classification schemes are simple but effective tools for attributing the impacts of climate change on ecosystems by combining the states of temperature and precipitation into one quantity (Feng et al., 2014). The Köppen climate classification was the first quantitative classification that empirically described the biome distribution of the Earth (Cui et al., 2021; Köppen, 1936). With modifications (Trewartha & Horn, 1980) and updates (Kottek et al., 2006; Peel et al., 2007), the Köppen climate classification has been used in numerous studies to show observed changes in the climate (C. Beck et al., 2005; Chan & Wu, 2015; D. Chen & Chen, 2013) and expected future changes based on the outputs of global climate model (GCM) projections (H. E. Beck et al., 2018; Feng et al., 2014; Mahlstein et al., 2013; Navarro et al., 2022).

Several of the latest generation of GCMs from Phase 6 of the Coupled Model Intercomparison Project (CMIP6; Eyring et al., 2016) show higher equilibrium climate sensitivities (ECS; representing the expected global warming following a doubling of atmospheric CO_2 compared to pre-industrial levels), than their predecessors in CMIP5 (Andrews et al., 2019; Forster et al., 2020; Gettelman et al., 2019; Golaz et al., 2019; Swart et al., 2019; Voldoire et al., 2019). The increase in the ECS in CMIP6 models is primarily attributed to positive cloud feedbacks and enhanced aerosol-cloud interactions (Meehl et al., 2020; Zelinka et al., 2020). The likely range of ECS (66%–100% probability) has been estimated at 1.5°C–4.5°C in the IPCC AR5 report (IPCC, 2013). However, the range has narrowed to 2.5°C–4°C in the latest AR6 report (IPCC, 2021), and the 5%–95% range is now estimated at 2.3°C–4.7°C (Sherwood et al., 2020). Some CMIP6 models with high ECS values have been criticized for simulating too strong warming that is unsupported by historical evidence (Tokarska et al., 2020; Zhu et al., 2020). Therefore, different approaches have been implemented to account for the so-called "hot model problem" (Hausfather et al., 2022), such as constraining the projections based on historical observations (Ribes et al., 2021; Tokarska et al., 2020) or weighting the models based on their performance and independence (Brunner et al., 2020; Liang et al., 2020). Although some models in CMIP6 may be less plausible due to their high ECS values outside the likely range, state-dependent cloud feedbacks could lead the climate system to a higher sensitivity state, making those higher ECS values plausible (Bjordal et al., 2020). Therefore, it is essential to evaluate the consequences of both the likely and less plausible but high-risk outcomes based on CMIP6 future climate projections, and to quantify their differences from expectations based on the previous generation of models in CMIP5.

In this study, we use observed global temperature and precipitation data along with CMIP5 and CMIP6 projections and apply the Köppen-Geiger climate classification (Peel et al., 2007) to analyze both observed and projected changes in climate zones from the beginning of the 20th century until the end of the 21st century and to highlight differences between the two model generations. We use historical CMIP5 and CMIP6 data to evaluate and compare their ability to replicate observed Köppen-Geiger climate classification maps (Gnanadesikan & Stouffer, 2006). We also use high-emission scenario future projections, the Shared Socioeconomic Pathway 5–8.5 (SSP5-8.5; Riahi et al., 2017) for CMIP6 and the Representative Concentration Pathway 8.5 (RCP8.5; van Vuuren et al., 2011) for CMIP5, to compare projections of future climate zone distributions both globally and at the continental level. We split the model generations into two subsets to address some CMIP6 models' tendency toward excessive warming for future climate state projections: the first subset contains models with better historical performance (without making any particular choice based on the ECS of the models) and the second subset contains the models that are consistent with the declared likely ECS range of 2.5°C–4°C (Hausfather et al., 2022). Finally, we look at the differences between their future rate of climate zone change projections and investigate the models' global mean land warming rates as the principal reason for the difference between the two model projections.

2. Data and Methods

2.1. Data

2.1.1. Observations and Reanalysis

This study uses two gridded observational data sets as the basis for the calculations: the Climatic Research Unit gridded Time Series v. 4.04 (CRU) monthly temperature data set (Harris et al., 2020) and the Global Precipitation Climatology Center (GPCC) monthly precipitation data set (Schneider et al., 2014), both of which are at 0.5° grid resolution. These two data sets, spanning 1901 to 2019 (GPCC extends back to 1891), are used to produce the past and present-day Köppen-Geiger climate classification maps for the 30-year periods 1901–1930 and

23284277, 2023, 4, Downloaded from https://agupubs.onlinelibrary.wiley.com/doi/10.1029/2022EF002972 by Ota Dogu Teknik Universitesi, Wiley Online Library on [20/10/2023]. See the Terms and Conditions (https://onlinelibrary.wiley.com/terms-and-conditions) on Wiley Online Library for rules of use; OA articles are governed by the applicable Creative Commons License

23284277, 2023, 4, Downloaded from https://agupubs.onlinelibrary.wiley.com/doi/10.1029/2022EF002972 by Ota Dogu Teknik Universitesi, Wiley Online Library on [20/10/2023]. See the Terms and Conditions (https://onlinelibrary.wiley.com/terms-and-conditions) on Wiley Online Library for rules of use; OA articles are governed by the applicable Creative Commons License

1990–2019, to evaluate GCM performance for the historical period 1976–2005 and to correct the mean biases of the GCMs. Throughout the study, Antarctica is excluded from the calculations due to the lack of sufficient observational data.

Analyses presented in the Results section use CRU temperature and GPCC precipitation as observational reference data sets. However, to investigate the uncertainty that might exist in these reference data sets and to measure the sensitivity of GCM performance to the reference data set, we have performed additional analyses utilizing other data sets as benchmarks, while their results are given in Figures S3–S9 in Supporting Information S1. Two additional temperature and precipitation data set couples are used. The first couple consists of the Global Historical Climatology Network version 2 and Climate Anomaly Monitoring System (GHCN-CAMS) monthly gridded temperature data set, covering the period from 1948 to 2019 (Fan & van den Dool, 2008), and the CRU monthly precipitation from 1901 to 2019 (Harris et al., 2020) data set (both at 0.5° resolution). The second couple is the ERA5 global reanalysis temperature and precipitation data (Hersbach et al., 2020) between 1959 and 2019 at 0.25° resolution. The ERA5 data have been regridded onto the common observational data grid resolution of 0.5° using bilinear interpolation.

Overall, the CRU temperature data set has good agreement with other observational and reanalysis data sets, such as CRUTEM4.6, UDEL, and JRA-55, with some differences in long-term trends (Harris et al., 2020). Even though the GPCC precipitation data set has large differences compared to the reanalysis data (e.g., ERA-40 and ERA-Interim; Schneider et al., 2014), it has very good agreement with the GPCP V2.2 precipitation data. Accordingly, in this study CRU and GPCC data sets are selected as the main observational reference for temperature and precipitation, respectively.

2.1.2. CMIP5 and CMIP6 GCMs

We use historical and future scenario simulations of monthly temperature and precipitation from 35 CMIP5 models (Taylor et al., 2012) and 33 CMIP6 models (Eyring et al., 2016); a complete list of the models can be found in Tables 1 and 2, respectively. Historical simulations span 1850 to 2005 (1850–2014) for CMIP5 (CMIP6), while future simulations cover the periods 2006–2100 (2015–2100) for CMIP5 (CMIP6). In this study, simulations from 1901 to 2100 have been used in the analyses. Only one variant (mostly r1i1p1 for CMIP5 and r1i1p1f1 for CMIP6) is considered for each model, as is the case for many previous studies (e.g., H. E. Beck et al., 2018; di Virgilio et al., 2022; Grose et al., 2020). All climate models have been downscaled onto the common grid of 0.5° resolution using bilinear interpolation prior to analysis. Historical simulations of the models have been used for evaluation against observations and for bias correction, while scenario simulations have been used to create the future Köppen-Geiger climate classification based analyses. For both sets of GCMs, high-emission scenarios have been used: the RCP8.5 (van Vuuren et al., 2011) for CMIP5 and the SSP5-8.5 (Riahi et al., 2017) for CMIP6. The SSP scenarios cover multiple baseline worlds facing different socioeconomic development challenges in the absence of new climate policies along with the climate forcing aspect of the RCPs (Riahi et al., 2017). Although both scenarios reach 8.5 W/m^2 radiative forcing by the end of the 21st century, disparities in their greenhouse gas and aerosol pathways lead to some differences in their projections that cannot be attributed to model behavior (Grose et al., 2020). However, the study of Tokarska et al. (2020) scaled the RCP8.5 warming by the SSP5-8.5 to RCP8.5 forcing ratio to estimate the CMIP5 response to the SSP scenario and found that the results are very similar to the original CMIP5 projections, suggesting that the stronger warming levels in CMIP6 are not substantially driven by differences between the scenarios.

The effective climate sensitivities for CMIP5 and CMIP6 GCMs given in Tables 1 and 2 are adopted from the study of Zelinka et al. (2020) to create likely model ensemble subsets (see Table 4) based on the IPCC's likely ECS range of 2.5°C–4°C (IPCC, 2021). The adopted values are generally for r1i1p1 (CMIP5) and r1i1p1f1 (CMIP6) variants. However, for the cases where the variants selected by the study of Zelinka et al. (2020) and our study do not match, the sensitivity values calculated in their study are assumed to be representative for the variant used here (there are only two models out of 68 for which the variants do not match; see Tables 1 and 2). Effective climate sensitivity values given by Zelinka et al. (2020) were calculated following Gregory et al. (2004)'s method using 150-year simulations, which has been shown to underestimate actual ECS (Rugenstein et al., 2020; Zelinka et al., 2020). Nevertheless, effective climate sensitivity is referred to as ECS throughout the paper, as it is common to use the terms interchangeably for simplicity.

Of the 35 (33) CMIP5 (CMIP6) models, there are 16 (11) models that fall within the likely ECS range (see asterisks marked in Tables 1 and 2). In this study, we have used these models, that is, 16 (11) CMIP5 (CMIP6) models, as likely model ensembles (Table 4) to investigate the projections representing more plausible future conditions.

23284277, 2023, 4, Downloaded from https://agupubs.onlinelibrary.wiley.com/doi/10.1029/2022EF002972 by Ota Dogu Teknik Universitesi, Wiley Online Library on [20/10/2023]. See the Terms and Conditions (https://onlinelibrary.wiley.com/terms-and-conditions) on Wiley Online Library for rules of use; OA articles are governed by the applicable Creative Commons License

Table 1
List of the Coupled Model Intercomparison Project Phase 5 (CMIP5) Global Climate Models Used in the Study, Along With Their Accuracies for the Reference Period 1976–2005 and Equilibrium Climate Sensitivities (ECS)

Model	Institution	Variant	ECS (K)	Accuracy (%)
ACCESS1-0*	CSIRO (Commonwealth Scientific and Industrial Research Organization), and BOM (Bureau of Meteorology)	r1i1p1	3.85	59.0
ACCESS1-3*		r1i1p1	3.55	57.5
BCC-CSM1-1*	Beijing Climate Center, China Meteorological Administration	r1i1p1	2.82	50.5
BCC-CSM1-1-m*		r1i1p1	2.89	50.9
BNU-ESM	College of Global Change and Earth System Science, Beijing Normal University	r1i1p1	4.04	51.1
CanESM2*	Canadian Center for Climate Modeling and Analysis	r1i1p1	3.70	52.9
CCSM4*	National Center for Atmospheric Research	r1i1p1	2.94	53.4
CESM1-BGC	National Science Foundation, Department of Energy, National Center for Atmospheric Research	r1i1p1		53.8
CESM1-CAM5		r1i1p1		57.6
CMCC-CESM	Centro Euro-Mediterraneo per I Cambiamenti Climatici	r1i1p1		54.1
CMCC-CMS		r1i1p1		57.8
CNRM-CM5*	Center National de Recherches Meteorologiques/Center Europeen de Recherche et Formation Avancees en Calcul Scientifique	r1i1p1	3.25	55.8
CSIRO-Mk3-6-0	Commonwealth Scientific and Industrial Research Organization in collaboration with the Queensland Climate Change Center of Excellence	r7i1p1	4.09 (r1i1p1)	51.2
FGOALS-g2*	LASG, Institute of Atmospheric Physics, Chinese Academy of Sciences; and CESS, Tsinghua University	r1i1p1	3.37	50.2
FIO-ESM	The First Institute of Oceanography, SOA	r1i1p1		52.3
GFDL-CM3*	Geophysical Fluid Dynamics Laboratory	r1i1p1	3.95	56.3
GFDL-ESM2G		r1i1p1	2.43	51.8
GFDL-ESM2M		r1i1p1	2.44	51.7
GISS-E2-H	NASA Goddard Institute for Space Studies	r1i1p1	2.31	51.6
GISS-E2-H-CC		r1i1p1		52.4
GISS-E2-R		r1i1p1	2.12	52.3
GISS-E2-R-CC		r1i1p1		52.1
HadGEM2-CC	Met Office Hadley Center	r1i1p1		56.5
INM-CM4	Institute for Numerical Mathematics	r1i1p1	2.08	48.0
IPSL-CM5A-MR	Institut Pierre-Simon Laplace	r1i1p1	4.11	54.2
IPSL-CM5B-LR*		r1i1p1	2.61	48.7
MIROC5*	Atmosphere and Ocean Research Institute (The University of Tokyo), National Institute for Environmental Studies, and Japan Agency for Marine-Earth Science and Technology	r1i1p1	2.71	51.1
MIROC-ESM	Japan Agency for Marine-Earth Science and Technology, Atmosphere and Ocean Research Institute (The University of Tokyo), and National Institute for Environmental Studies	r1i1p1	4.65	45.8
MIROC-ESM-CHEM		r1i1p1		46.2
MPI-ESM-LR*	Max Planck Institute for Meteorology (MPI-M)	r1i1p1	3.63	60.1
MPI-ESM-MR*		r1i1p1	3.45	60.0
MRI-CGCM3*	Meteorological Research Institute	r1i1p1	2.61	59.0
MRI-ESM1		r1i1p1		59.4
NorESM1-M*	Norwegian Climate Center	r1i1p1	2.87	50.2
NorESM1-ME*		r1i1p1	2.98	50.1

Note. Models in bold are the selected 25 CMIP5 models with the highest accuracies, while the rest are discarded from the CMIP5 multi-model ensemble. ECS values calculated for a different ensemble member by Zelinka et al. (2020) than the member we used are indicated in parentheses. The models that fall within the likely ECS range of 2.5°C–4°C (IPCC, 2021), and hence selected for the likely ensemble subset, are marked with an asterisk (*).

Table 2
List of the Coupled Model Intercomparison Project Phase 6 (CMIP6) Global Climate Models Used in the Study, Along With Their Accuracies for the Reference Period 1976–2005 and Equilibrium Climate Sensitivities (ECS)

Model	Institution	Variant	ECS (K)	Accuracy (%)
ACCESS-CM2	Commonwealth Scientific and Industrial Research Organization; Australian Research Council Center of Excellence for Climate System Science	r1i1p1f1	4.66	57.2
ACCESS-ESM1-5*	Commonwealth Scientific and Industrial Research Organization	r1i1p1f1	3.88	57.4
BCC-CSM2-MR*	Beijing Climate Center	r1i1p1f1	3.02	54.3
CAMS-CSM1-0	Chinese Academy of Meteorological Sciences	r1i1p1f1	2.29	51.7
CanESM5	Canadian Center for Climate Modeling and Analysis	r1i1p1f1	5.64	56.0
CanESM5-CanOE		r1i1p2f1		56.5
CESM2	National Center for Atmospheric Research, Climate and Global Dynamics Laboratory	r4i1p1f1	5.15 (r1i1p1f1)	62.4
CESM2-WACCM		r1i1p1f1	4.68	61.4
CMCC-CM2-SR5*	Fondazione Centro Euro-Mediterraneo sui Cambiamenti Climatici	r1i1p1f1	3.55	59.2
CMCC-ESM2*		r1i1p1f1	3.58	60.1
CNRM-CM6-1	Center National de Recherches Meteorologiques; Center Europeen de Recherche et de Formation Avancee en Calcul Scientifique	r1i1p1f2	4.90	57.3
E3SM-1-1	E3SM-Project: Lawrence Livermore National Laboratory; Argonne National Laboratory; Brookhaven National Laboratory; Los Alamos National Laboratory; Lawrence Berkeley National Laboratory; Oak Ridge National Laboratory; Pacific Northwest National Laboratory; Sandia National Laboratories	r1i1p1f1		55.6
EC-Earth3-CC	EC-Earth-Consortium	r1i1p1f1	4.23	65.5
FGOALS-f3_L*	Chinese Academy of Sciences	r1i1p1f1	2.98	51.0
FGOALS-g3*		r1i1p1f1	2.87	43.6
FIO-ESM-2-0	First Institute of Oceanography; Qingdao National Laboratory for Marine Science and Technology	r1i1p1f1		60.0
GFDL-ESM4*	National Oceanic and Atmospheric Administration, Geophysical Fluid Dynamics Laboratory	r1i1p1f1	2.65	61.6
HadGEM3-GC31-LL	Met Office Hadley Center; Natural Environment Research Council	r1i1p1f3	5.55	63.0
HadGEM3-GC31-MM	Met Office Hadley Center	r1i1p1f3	5.44	67.3
IITM-ESM	Center for Climate Change Research, Indian Institute of Tropical Meteorology	r1i1p1f1	2.37	54.9
INM-CM4-8	Institute for Numerical Mathematics, Russian Academy of Science	r1i1p1f1	1.83	52.4
INM-CM5-0		r1i1p1f1	1.92	54.6
IPSL-CM6A-LR	Institut Pierre Simon Laplace	r1i1p1f1	4.70	56.8
KACE-1-0-G	National Institute of Meteorological Sciences/Korea Meteorological Administration	r1i1p1f1	4.75	56.5
MCM-UA-1-0	Department of Geosciences, University of Arizona	r1i1p1f2		45.8
MIROC6*	Japan Agency for Marine-Earth Science and Technology; Atmosphere and Ocean Research Institute, The University of Tokyo; National Institute for Environmental Studies; RIKEN Center for Computational Science	r1i1p1f1	2.60	53.4
MIROC-ES2L*		r1i1p1f2	2.66	50.4
MPI-ESM1-2-LR*	Max Planck Institute for Meteorology; Alfred Wegener Institute, Helmholtz Center for Polar and Marine Research; Deutsches Klimarechenzentrum; Deutscher Wetterdienst	r1i1p1f1	3.03	56.6
MRI-ESM2-0*	Meteorological Research Institute	r1i1p1f1	3.13	63.5
NESM3	Nanjing University of Information Science and Technology	r1i1p1f1	4.76	53.1
NorESM2-MM	NorESM Climate modeling Consortium	r1i1p1f1	2.49	59.3
TaiESM1	Research Center for Environmental Changes, Academia Sinica	r1i1p1f1	4.36	59.8
UKESM1-0-LL	Met Office Hadley Center; Natural Environment Research Council; National Institute of Meteorological Sciences/Korea Meteorological Administration; National Institute of Water and Atmospheric Research	r1i1p1f2	5.36	61.8

Note. Models in bold are the selected 25 CMIP6 models with the highest accuracies, while the rest are discarded from the CMIP6 multi-model ensemble. ECS values calculated for a different ensemble member by Zelinka et al. (2020) than the member we used are indicated in parentheses. The models that fall within the likely ECS range of 2.5°C–4°C (IPCC, 2021), and hence selected for the likely ensemble subset, are marked with an asterisk (*).

23284277, 2023, 4, Downloaded from https://agupubs.onlinelibrary.wiley.com/doi/10.1029/2022EF002972 by Orta Dogu Teknik Universitesi, Wiley Online Library on [20/10/2023]. See the Terms and Conditions (https://onlinelibrary.wiley.com/terms-and-conditions) on Wiley Online Library for rules of use; OA articles are governed by the applicable Creative Commons License

23284277, 2023, 4, Downloaded from https://agupubs.onlinelibrary.wiley.com/doi/10.1029/2022EF002972 by Ota Dogu Teknik Universitesi, Wiley Online Library on [20/10/2023]. See the Terms and Conditions (https://onlinelibrary.wiley.com/terms-and-conditions) on Wiley Online Library for rules of use; OA articles are governed by the applicable Creative Commons License

Table 3
Defining Criteria of the Köppen-Geiger Climate Classification, Adapted From Peel et al. (2007)

1st	2nd	3rd	Description	Criteria[a]
A			Tropical	$T_{cold} \geq 18$
	f		Rainforest	$P_{dry} \geq 60$
	m		Monsoon	Not (Af) and $P_{dry} \geq 100–MAP/25$
	w		Savannah	Not (Af) and $P_{dry} < 100–MAP/25$
B			Arid	$MAP < 10 \times P_{threshold}$
	W		Desert	$MAP < 5 \times P_{threshold}$
	S		Steppe	$MAP \geq 5 \times P_{threshold}$
		h	Hot	$MAT \geq 18$
		k	Cold	$MAT < 18$
C			Temperate	$T_{hot} > 10$ and $0 < T_{cold} < 18$
	s		Dry Summer	$P_{sdry} < 40$ and $P_{sdry} < P_{wwet}/3$
	w		Dry Winter	$P_{wdry} < P_{swet}/10$
	f		Without dry season	Not (Cs) or (Cw)
		a	Hot Summer	$T_{hot} \geq 22$
		b	Warm Summer	Not (a) and $T_{mon10} \geq 4$
		c	Cold Summer	Not (a or b) and $1 \leq T_{mon10} < 4$
D			Cold	$T_{hot} > 10$ and $T_{cold} \leq 0$
	s		Dry Summer	$P_{sdry} < 40$ and $P_{sdry} < P_{wwet}/3$
	w		Dry Winter	$P_{wdry} < P_{swet}/10$
	f		Without dry season	Not (Ds) or (Dw)
		a	Hot Summer	$T_{hot} \geq 22$
		b	Warm Summer	Not (a) and $T_{mon10} \geq 4$
		c	Cold Summer	Not (a, b or d)
		d	Very Cold Winter	Not (a or b) and $T_{cold} < -38$
E			Polar	$T_{hot} < 10$
	T		Tundra	$T_{hot} > 0$
	F		Frost	$T_{hot} \leq 0$

[a]T_{cold} = Temperature of the coldest month, P_{dry} = Precipitation of the driest month, MAP = Mean annual precipitation, MAT = Mean annual temperature, T_{hot} = Temperature of the hottest month, P_{sdry} = Precipitation of the driest month in summer, P_{wwet} = Precipitation of the wettest month in winter, P_{wdry} = Precipitation of the driest month in winter, P_{swet} = Precipitation of the wettest month in summer, T_{mon10} = Number of months where the temperature is above 10, $P_{threshold}$ depends on conditions: $P_{threshold} = 2 \times MAT$ if 70% of MAP occurs in winter, $P_{threshold} = 2 \times MAT + 28$ if 70% of MAP occurs in summer, $P_{threshold} = 2 \times MAT + 14$ otherwise. Summer (winter) is the warmer (colder) of the two 6-month periods, October–March or April–September.

2.2. Methods

2.2.1. Köppen-Geiger Climate Classification

We use the updated version of the Köppen-Geiger climate classification as explained in detail in Peel et al. (2007). The calculation scheme for obtaining the respective climate classes is given in Table 3. Throughout the study, Köppen-Geiger climate zones are calculated using 30-year time slices of monthly temperature and precipitation data.

2.2.2. Evaluation of GCM Performance

Comparison of the climate model simulations against observations can be utilized as a diagnostic tool to evaluate the change in model accuracy between the model generations (Flato et al., 2013). Several previous studies conducted at regional scales have reported incremental improvements in the CMIP6 models' capability

23284277, 2023, 4, Downloaded from https://agupubs.onlinelibrary.wiley.com/doi/10.1029/2022EF002972 by Orta Dogu Teknik Universitesi, Wiley Online Library on [20/10/2023]. See the Terms and Conditions (https://onlinelibrary.wiley.com/terms-and-conditions) on Wiley Online Library for rules of use; OA articles are governed by the applicable Creative Commons License

Table 4
Description of the Ensemble Subsets Used Throughout the Study

Ensemble name	Number of models included	Method
CMIP5 ensemble[a]	25	25 CMIP5 models with the highest accuracy (Equation 1)
CMIP6 ensemble[a]	25	25 CMIP6 models with the highest accuracy (Equation 1)
CMIP5 likely ensemble	16	CMIP5 models whose ECS lie in the likely range of 66%–100% probability, that is 2.5°C–4°C (IPCC, 2021)
CMIP6 likely ensemble	11	CMIP6 models whose ECS lie in the likely range of 66%–100% probability, that is 2.5°C–4°C (IPCC, 2021)

[a]To prevent confusion between different ensemble subsets, Coupled Model Intercomparison Project Phase 5 (CMIP5) and Coupled Model Intercomparison Project Phase 6 (CMIP6) ensembles are sometimes referred to as 25-member ensembles throughout the text.

to represent the observed climatology of mean temperature and precipitation (Bağçaci et al., 2021; Grose et al., 2020; Lun et al., 2021; Ortega et al., 2021), as compared to CMIP5. In this study, we compare the accuracy of Köppen-Geiger climate classification maps obtained using the two generations of climate models, CMIP5 and CMIP6, against observation-based maps for the reference periods (1976–2005, 1961–1990, and 1990–2019) to evaluate their performance.

Having all model and observational data at the same spatial resolution (0.5°), the climate models' skill in replicating the reference period Köppen-Geiger climate classification map is measured in terms of the correctly assigned percentage of total land area based on corresponding grid cells:

$$\text{Accuracy} = \frac{\sum_{i=1}^{n_a} A_i}{\sum_{i=1}^{n_t} A_i} \times 100 \quad (1)$$

where n_a is the total number of grid cells over land where the climate model and observations agree on the assigned climate class, n_t is the total number of grid cells over land areas and A_i is the area of each corresponding grid cell.

As a result of this evaluation process, the 25 CMIP5 and 25 CMIP6 models with the highest accuracies have been selected to use as the other ensemble subset in addition to the "likely model" ensemble (models are listed in Tables 1 and 2; selection criteria are listed in Table 4). Here, the number 25 is arbitrarily selected to ensure ensemble size-based sampling uncertainties for CMIP5 and CMIP6 are the same and to retain a higher number of models than those eliminated.

2.2.3. Production of the GCM-Based Köppen-Geiger Climate Classification Maps

GCM data contain systematic biases, which manifest as deviations from the historical observed climatology (Mehrotra & Sharma, 2015; Papadimitriou et al., 2017). Here, to correct the mean biases in the climate projections, a simple mean bias correction (Maraun, 2016) has been applied for CMIP5 and CMIP6 historical and future temperature and precipitation simulations (corrected historical GCMs were only used for the change rate calculations and not for performance evaluation). During the bias correction calculations, the 1976–2005 monthly temperature and precipitation observations were taken as the reference (for details on the bias correction method, please see Text S1 in Supporting Information S1).

By using the bias-corrected climate projections of CMIP5 and CMIP6 models, a separate Köppen-Geiger climate classification map has been created for each model for each time period of interest. Then, four different ensemble subsets have been created, for which the details are given in Table 4. For each subset, an additional map has been created by selecting the most frequent climate class for each grid cell among the climate classifications of all models (H. E. Beck et al., 2018). Consequently, a total of four global Köppen-Geiger climate classification maps were created based on these four model ensemble subsets. These form the basis of the climate classification analyses representing the ensembles.

To determine the historical accuracy of the GCMs based on the Köppen-Geiger climate classifications, two maps have been created for the 1976–2005 period using the most frequent climate class approach for the CMIP5 and CMIP6 ensembles, and their accuracies have been calculated using Equation 1. Grid cells that are assigned

23284277, 2023, 4, Downloaded from https://agupubs.onlinelibrary.wiley.com/doi/10.1029/2022EF002972 by Ota Dogu Teknik Universitesi, Wiley Online Library on [20/10/2023]. See the Terms and Conditions (https://onlinelibrary.wiley.com/terms-and-conditions) on Wiley Online Library for rules of use; OA articles are governed by the applicable Creative Commons License

to different climate classes for climate model-based and observation-based reference maps are referred to as "mismatches".

The methodology used to create the "ensemble maps" also enables measurement of the level of consistency between the GCMs for the future period (2071–2100) (H. E. Beck et al., 2018). Level of consistency (*L.o.c.*) is defined for a grid cell as:

$$L.o.c. = \frac{N_f}{N_t} \times 100 \tag{2}$$

where N_f is the frequency of the most frequent climate class for that grid cell on the climate model ensemble and N_t is the total number of models in the ensemble. Then, global level of consistencies for CMIP5 and CMIP6 are calculated by taking area-weighted averages of level of consistencies for all grid cells over the land areas.

2.2.4. Temperature Anomalies

Global mean surface temperature (land and ocean) between 2001 and 2020 has been observed to be 0.99°C higher than the average between 1850 and 1900 (90% confidence interval: 0.84 to 1.10), with larger increases over land areas than oceans (IPCC, 2021). We have calculated the temperature anomalies over each land climate zone by subtracting the area-weighted average temperatures (because grid cells have different areas over the different locations) between the two time frames:

$$\Delta T_i = \mu(T_i)_{\text{time slice}_2} - \mu(T_i)_{\text{time slice}_1} \tag{3}$$

where ΔT_i is the temperature difference over the climate zone, $\mu(T_i)$ is the average temperature over the climate zone, i is the accompanying climate zone (30 in total, from Af to EF) of the base period, time slice$_2$ is the latter time period of 30 years, and time slice$_1$ is the former time period of 30 years.

To calculate future temperature anomalies, we obtain two bias-corrected multi-model ensemble means (one for CMIP5 and one for CMIP6) for the end of the century (2071–2100) using the 25 models with the highest accuracies (these ensemble means are different than the previously mentioned ensemble maps, as the frequency approach cannot be used here).

2.2.5. Rate of Climate Zone Change

We define the rate of climate zone change as the total land area changing its climate zone per year between two consecutive 30-year time frames. To calculate the rate of climate zone change, we have obtained global Köppen-Geiger climate classification maps starting from the beginning of the 20th century until the end of the 21st century, using 30-yearly time slices of monthly climate data sets as input for each map. Maps are created by shifting the 30-year input window at 5-year intervals (e.g., 1901–1930, 1906–1935, 1911–1940, …, 2071–2100). The change rate of the climate zones over the Earth's land area is defined as:

$$\text{Change rate} = \frac{\sum_{j=1}^{n_c} A_j}{\Delta Y} \tag{4}$$

where n_c is the total number of grid cells over land areas changing their climate zones between two consecutive 30-year time frames (e.g., climate zones of 1901–1930 vs. 1931–1960), ΔY is the time difference between the middle years of the two periods (30 years in this case), and A_j is the area of the corresponding grid cell. The calculated change rate is assigned to the middle year of the second time frame (1945 for this example).

Loss rates of major climate zones were obtained in a similar way to the change rates of climate zones, but the total lost area of any given major climate zone was divided by the total area of that climate zone in the base period to obtain a percentage change. Finally, previously obtained 30-year Köppen-Geiger global maps with 5-year intervals were also used to obtain the areal coverage of each major climate zone as a time series with 5-year time steps.

To determine total land area changing its climate zone as a function of global mean land warming, we first brought all individual models to the same global land warming threshold levels (e.g., 1°C, 1.5°C, 2°C) relative to the baseline period observations (1901–1930). Then, using the ensemble models obtained with the frequency approach for each warming level, we calculated the total land area for the grids that have changed their climate zones ($\sum_{j=1}^{n_c} A_j$) relative to the baseline period observations.

23284277, 2023, 4, Downloaded from https://agupubs.onlinelibrary.wiley.com/doi/10.1029/2022EF002972 by Orta Dogu Teknik Universitesi, Wiley Online Library on [20/10/2023]. See the Terms and Conditions (https://onlinelibrary.wiley.com/terms-and-conditions) on Wiley Online Library for rules of use; OA articles are governed by the applicable Creative Commons License

Throughout the calculations of the rate of change, loss rates, and total land areas, bias-corrected historical and future simulations of CMIP5 and CMIP6 models have been used (1901–2100) with the observational data (1901–2019).

2.2.6. Confidence Intervals

Confidence intervals were estimated by applying a non-parametric bootstrap method (Efron, 1979), sampling across models creating 1000 sets of model ensemble realizations. After choosing the relevant number of ensemble members (e.g., 11 models for CMIP6 likely ensemble, 16 models for CMIP5 likely ensemble, or 25 models for CMIP5 and CMIP6 ensembles), each set of ensemble realizations has been obtained by random selection of models allowing for replacement. Then, all analyses in the study have been repeated with those samples (by obtaining a most frequent climate class-based estimate for each realization). Finally, using all 1000 realizations, 2.5% and 97.5% quantiles were taken as the upper and lower bounds for the 95% confidence interval.

3. Results

3.1. Köppen-Geiger Climate Classification Maps

Figure 1 shows the global distribution of the climate zones for the past (1901–1930), observed shifts in present-day climate (1990–2019) from the past, and projected future (2071–2100) shifts from the present-day climate based on CMIP5 and CMIP6 ensembles. Overall, the change between the observed climate classification maps during the early 20th and 21st centuries (Figure 1b) is considerably less than the projected change between the early and late 21st centuries for both CMIP5 and CMIP6 ensembles (Figures 1c and 1d). The projected changes in climate zones by the end of the century are more extensive in the CMIP6 ensemble than in CMIP5, especially over the cold climate zones in the high latitudes of the Northern Hemisphere (Figure 1e; and global maps showing the distributions of the climate zones for GCM ensembles and observational data are shown in Figure S1 in Supporting Information S1).

A question might arise whether the results are sensitive to the choice of the reference data set (CRU and GPCC for temperature and precipitation, respectively). We have investigated the consistency of the climate maps with two additional data sets (GHCN-CAMS/CRU and ERA5/ERA5 for temperature/precipitation) for the present-day conditions (Figures S6 and S7 in Supporting Information S1). Present-day observed Köppen-Geiger maps show some differences, especially over Siberia, mountainous regions, and at the boundaries of climate zones, depending on the observation data used. Overall, CRU/GPCC versus ERA5 areal overlap is 76.9%, CRU/GPCC versus GHCN-CAMS/CRU is 80.4%, and ERA5 versus GHCN-CAMS/CRU is 76.2%. Accordingly, CRU/GPCC has a slightly higher average overlap against other products (78.65%) than ERA5 (76.55%) and GHCN-CAMS/CRU (78.3%).

Of the 25 models in the CMIP6 ensemble (Table 2), 12 models exhibit higher ECS than the IPCC's likely range of 2.5°C–4°C (IPCC, 2021); hence, the climate classifications differ somewhat. Namely, for CMIP6 (CMIP5), the average ECS value of likely ensemble is 3.09 K (3.20 K), while for 25-member ensemble the average is 4.05 K (3.20 K) (Tables 1 and 2). Accordingly, we have determined the projections based on likely ensembles to better understand the effects of higher ECS models on climate zone distributions. The likely model projections for the Köppen-Geiger climate zones by the end of the century for CMIP5 and CMIP6 (Figure 2) are more consistent with each other than the 25-member ensembles (Figures 1c–1e): 90.55% of the land areas overlap for the likely model ensembles, whereas it is about 79.08% for the 25-member ensembles (global maps showing the climate zone distributions for likely GCM ensembles are shown in Figure S2 in Supporting Information S1). Also, the apparent differences observed over the higher latitudes between CMIP5 and CMIP6 ensembles almost vanish for the difference between likely ensembles (Figure 2d). However, some CMIP6 models in the likely model ensemble have low climate classification accuracies (e.g., FGOALS-g3 in Table 2), while some models with ECS values outside the likely range have high accuracies (e.g., HadGEM3-GC31-MM in Table 2). Therefore, a joint investigation of the distribution of the climate zones based on the accuracy-based ensemble (i.e., 25-member ensemble) along with the likely model ensemble is valuable. A better approach might be treating the CMIP6 ensemble as a lower likelihood but higher risk projection and the likely ensemble as the more plausible projection.

3.2. Performance of CMIP5 and CMIP6 Climate Classifications

The accuracies (Equation 1) of individual climate classification maps are calculated for both CMIP5 and CMIP6 ensembles for the reference period 1976–2005. The correctly identified grid cell ratios of CMIP6 models are on

10.1029/2022EF002972

23284277, 2023, 4, Downloaded from https://agupubs.onlinelibrary.wiley.com/doi/10.1029/2022EF002972 by Orta Dogu Teknik Universitesi, Wiley Online Library on [20/10/2023]. See the Terms and Conditions (https://onlinelibrary.wiley.com/terms-and-conditions) on Wiley Online Library for rules of use; OA articles are governed by the applicable Creative Commons License

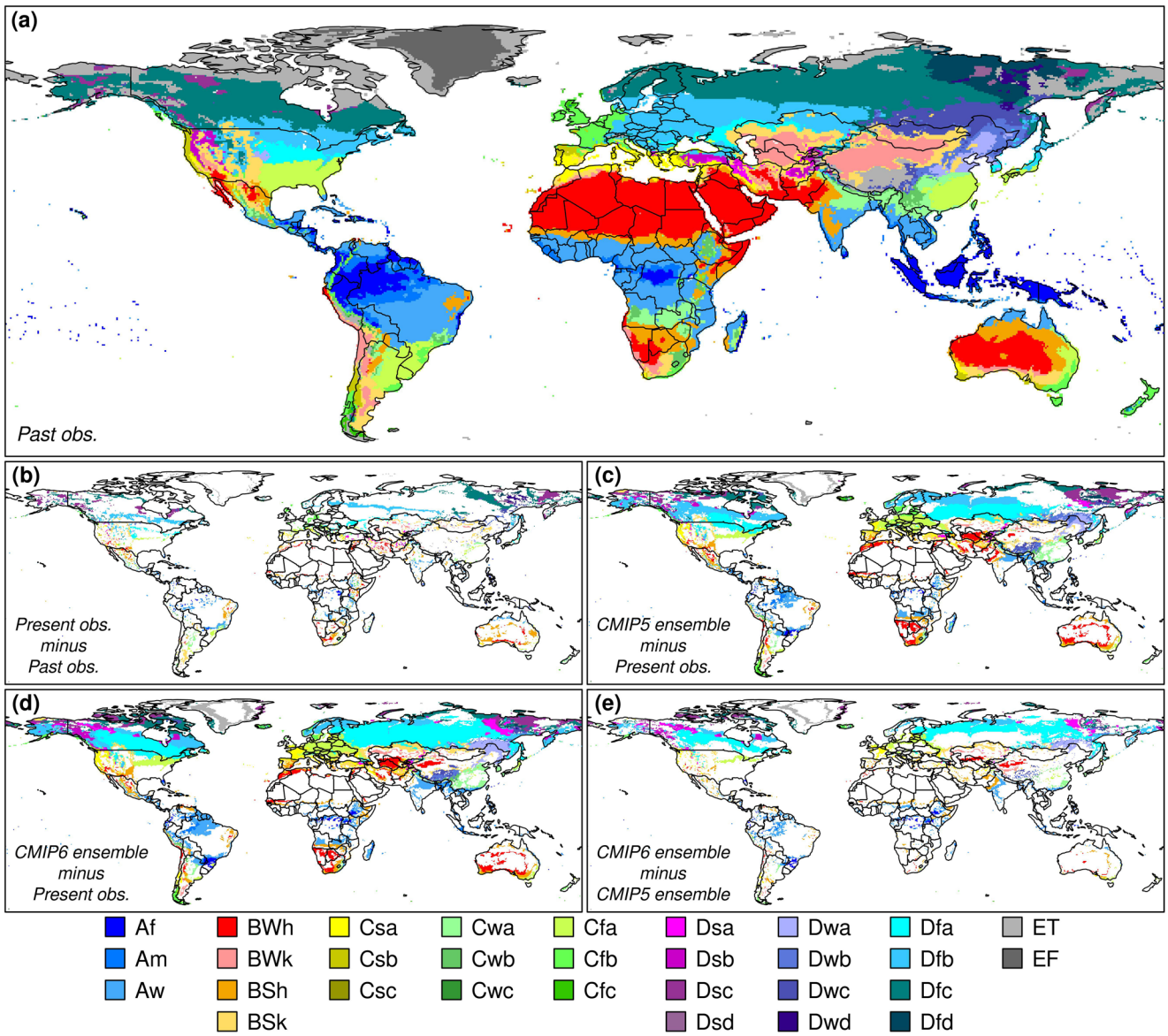

Figure 1. Köppen-Geiger climate classification maps based on (a) the early 20th century (1901–1930) observations (Climatic Research Unit temperature and Global Precipitation Climatology Center precipitation), (b) the difference between observed present-day (1990–2019) and past (1901–1930), (c) the difference between the future (2071–2100) Coupled Model Intercomparison Project Phase 5 (CMIP5) ensemble (25 models) and present-day observations, (d) the difference between the future Coupled Model Intercomparison Project Phase 6 (CMIP6) ensemble (25 models) and present-day observations, (e) the difference between the future CMIP6 and CMIP5 ensembles. The color scheme is adapted from Peel et al. (2007).

average (59.13% [whole range for the 25 models with the highest accuracies: 54.30–67.33]) higher than CMIP5 (54.95% [51.11–60.10]) as shown in Figure 3e. When the ensemble model maps are used, the accuracies of both model generations increase, but the relative performance for the correct classification of CMIP6 (65.34%) becomes only marginally better than CMIP5 (63.74%) (Figures 3a and 3b). This implies that although individual CMIP6 model simulations generally yield higher classification accuracies than CMIP5, the rate of improvement reduces when the ensemble information obtained from these model generations is used in the context of climate classifications. Nevertheless, the improved performance observed in CMIP6 versus CMIP5 is not sensitive to the choice of the reference data set or the period, as CMIP6 slightly but consistently performs better (Figures S8 and S9 in Supporting Information S1). These accuracy estimates are lower than those obtained in previous studies using CMIP5 simulations (Belda et al., 2015; Phillips & Bonfils, 2015), likely because we have used a larger number of climate classes to calculate the accuracy estimates than previous studies.

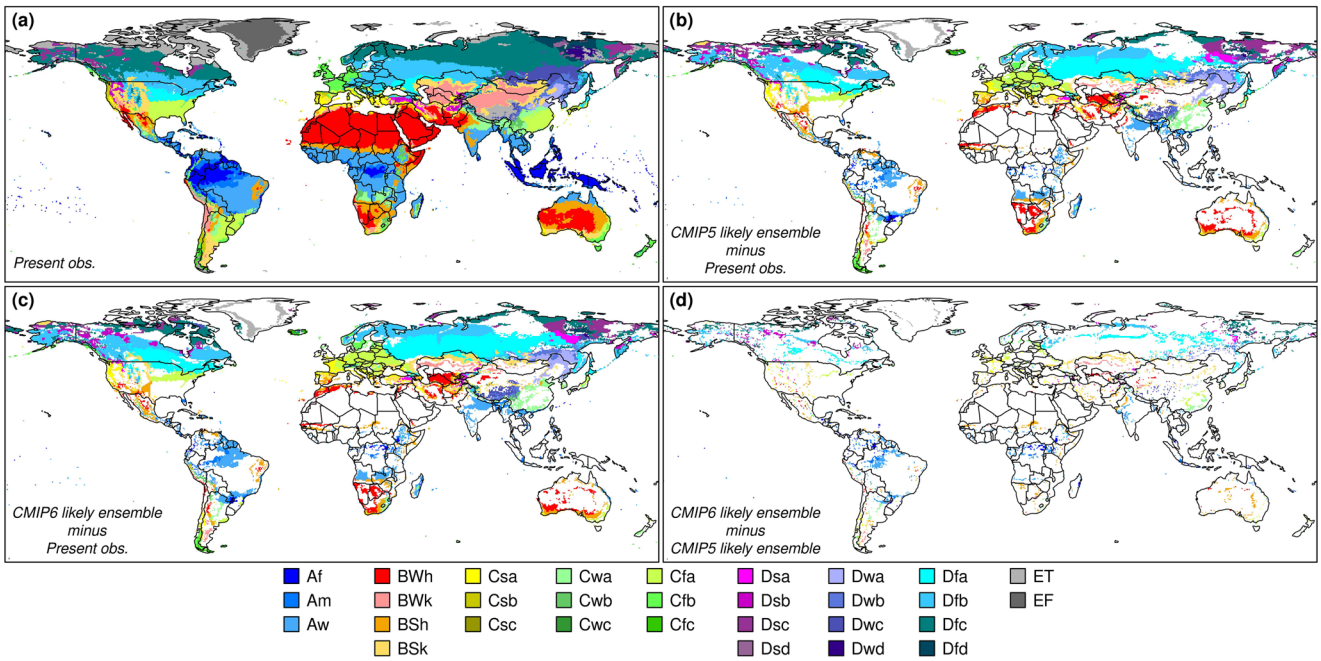

Figure 2. Köppen-Geiger climate classification maps based on (a) present-day (1990–2019) observations (Climatic Research Unit temperature and Global Precipitation Climatology Center precipitation), (b) the difference between the future (2071–2100) Coupled Model Intercomparison Project Phase 5 (CMIP5) likely ensemble and present-day observations, (c) the difference between the future Coupled Model Intercomparison Project Phase 6 (CMIP6) likely ensemble and present-day observations, (d) the difference between the future CMIP6 and CMIP5 likely ensembles.

Although the ability to represent the historical climate in the ensemble maps is marginally improved in CMIP6 models compared to CMIP5, the regions that are misidentified by CMIP5 and CMIP6 models for the reference period are very similar, such as the west coasts of North and South America, Amazonia, central Australia, southern Africa and Siberia, in addition to the regions of boundaries between climate zones (Figures 3a and 3b). CMIP5 simulations have been reported to have temperature biases over high elevations of the Himalayas, Greenland, and over ocean upwelling regions off the west coasts of South America and Africa (Flato et al., 2013). Also, most of the CMIP5 models have been shown to overestimate precipitation over regions with complex topography (Mehran et al., 2014) and some underestimate rainfall over Amazonia (Yin et al., 2013). Biases in the ensemble mean temperature and precipitation of CMIP6 are lower than for CMIP5 for the reference period 1976–2005 (6.44% reduction in 30-year mean temperature bias and 3.29% reduction in 30-year mean precipitation bias), while previously mentioned regional bias patterns remain (Figures 3c and 3d). The models' regional temperature and precipitation biases against observations lead to misclassifications in their Köppen-Geiger climate classification maps. Therefore, not surprisingly, regions with large temperature or precipitation biases, such as the west coasts of America, Himalayas, Amazonia, and Siberia (CMIP6: Figures 3c and 3d, CMIP5: Figure S10 in Supporting Information S1), have misclassified climate zones and lower climate classification accuracies (Figures 3a and 3b). Nevertheless, some biases in the models do not lead to misclassifications in the Köppen-Geiger maps, such as the cold bias over a large portion of Greenland (Figure 3c). This is because of the threshold-based nature of the Köppen-Geiger climate classification; colder simulated temperatures for a region already in the polar frost (EF) climate zone do not affect its classification. On the other hand, for some regions of Earth, ensemble mean biases and climate classifications based on the frequency method might not be correlated, such as over Australia. Most of the bias patterns are shared across the two model generations, but there are also regional differences. Some examples are reduced warm bias over Northern Canada and aggravated wet bias over the western coasts of Peru and Ecuador in CMIP6 versus CMIP5 (detailed differences between the historical simulations of the two model generations can be seen in Figure S11 in Supporting Information S1).

Inter-model consistency between the future projections of the Köppen-Geiger climate classification maps can be interpreted as an estimate of their future confidence levels. Future (2071–2100) CMIP6 climate classification level of consistency (global average of 79.18%; Figure S12b in Supporting Information S1) is slightly lower than that for CMIP5 (80.06%; Figure S12a in Supporting Information S1), with similar patterns to those observed

23284277, 2023, 4, Downloaded from https://agupubs.onlinelibrary.wiley.com/doi/10.1029/2022EF002972 by Orta Dogu Teknik Universitesi, Wiley Online Library on [20/10/2023]. See the Terms and Conditions (https://onlinelibrary.wiley.com/terms-and-conditions) on Wiley Online Library for rules of use; OA articles are governed by the applicable Creative Commons License

10.1029/2022EF002972

23284277, 2023, 4, Downloaded from https://agupubs.onlinelibrary.wiley.com/doi/10.1029/2022EF002972 by Orta Dogu Teknik Universitesi, Wiley Online Library on [20/10/2023]. See the Terms and Conditions (https://onlinelibrary.wiley.com/terms-and-conditions) on Wiley Online Library for rules of use; OA articles are governed by the applicable Creative Commons License

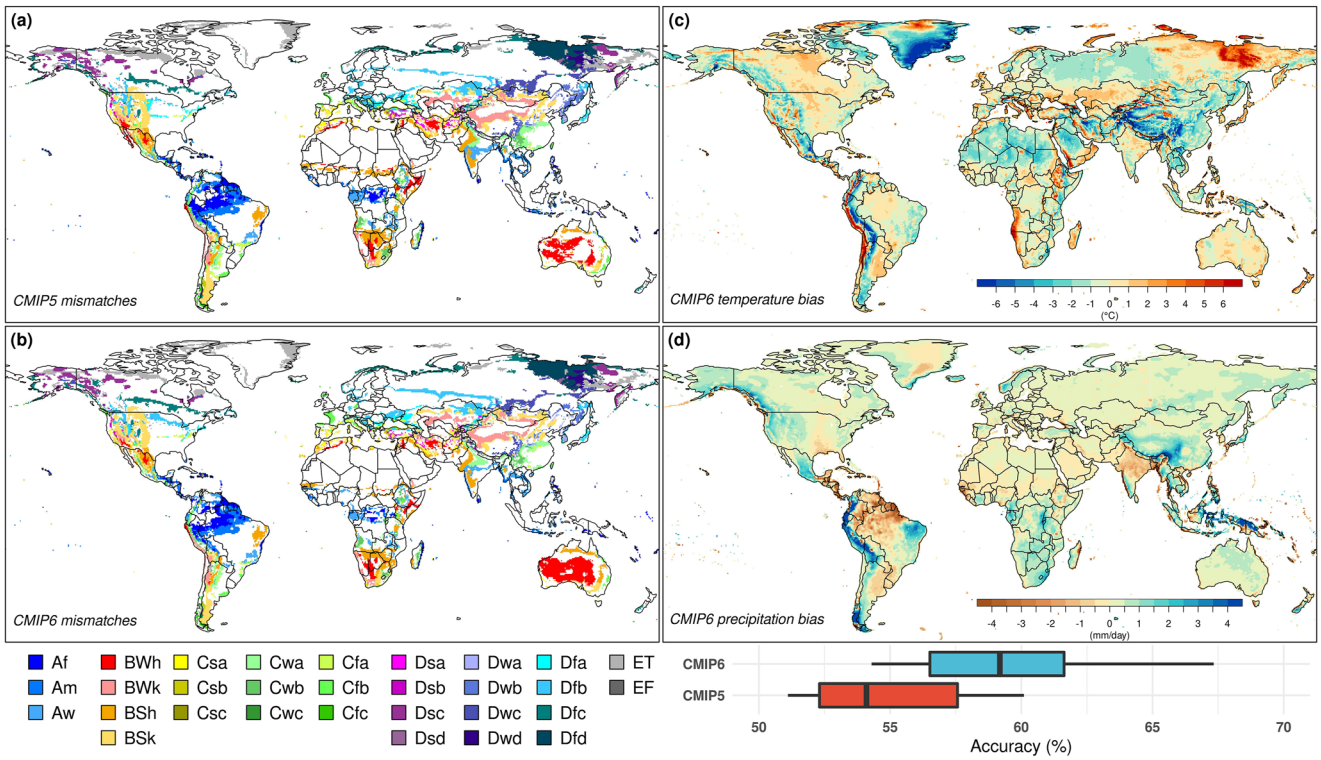

Figure 3. Historical climate classification accuracies of Coupled Model Intercomparison Project Phase 5 (CMIP5) and Coupled Model Intercomparison Project Phase 6 (CMIP6) ensembles, and reference period temperature and precipitation bias of the CMIP6 ensemble mean. (a) Regions where the CMIP5 ensemble inaccurately simulated the reference period (1976–2005) climate zones relative to the observations, defined as mismatches (disagreement on the assigned climate class) between the CMIP5 ensemble map and observed map. Colored regions show the locations of mismatches and colors are selected to be consistent with the observation-based map. (b) Same as (a) but using the CMIP6 ensemble map. (c) CMIP6 historical ensemble mean annual mean temperature bias with respect to the reference period observations. (d) CMIP6 historical ensemble mean annual precipitation bias with respect to the reference period observations, in mm/day. (e) The distribution of the global mean accuracies (i.e., the globally averaged percentage of correctly assigned area) for classification maps derived individually from the 25 CMIP5 and 25 CMIP6 models for the reference period.

in the historical period. Moreover, consistencies become lower toward the higher latitudes, as also found in the H. E. Beck et al. (2018). Although the overall scores and general patterns of the future level of consistencies for the two model generations are similar, some regional differences exist, as is the case with historical biases. For example, CMIP6 models show a higher future level of consistency than CMIP5 in central Russia but a lower level of consistency in northern Russia.

3.3. CMIP5 and CMIP6 Future Temperature Anomalies

We calculate the observed temperature anomalies between 1990–2019 and 1901–1930 over each Köppen-Geiger climate zone: Cwc has experienced the least amount of warming (0.21°C), and Dsd has experienced the greatest amount of warming (1.86°C), with the global mean land surface temperature increase of 0.95°C (Figure S13 in Supporting Information S1). Projections of the least and the most severe warming climate zones by the end of the century are consistent across different climate model ensembles: Cfc and Dfd (Figure S14 in Supporting Information S1). However, the range of the projected warming changes sharply across the ensembles. The CMIP5 RCP8.5 ensemble mean projects a global mean land warming of 4.29°C [95% confidence interval: 3.93–4.66] by the end of the century relative to the present-day (Figure S14a in Supporting Information S1). On the other hand, mean warming reduces to 3.82°C [3.49–4.16] when the likely CMIP5 model subset is used (Figure S14b in Supporting Information S1). This difference between the two ensemble subsets becomes more prominent for CMIP6: the ensemble mean projects 5.64°C [5.11–6.20] of warming (Figure S14c in Supporting Information S1), while the likely model ensemble mean projects 4.45°C [4.09–4.80] by the end of the century relative to present-day observations (Figure S14d in Supporting Information S1). The sharper decline in the mean projected warming and uncertainty range from the CMIP6 ensemble to the CMIP6 likely ensemble compared to the difference between the CMIP5 ensembles is due to the preponderance of the high sensitivity models in the CMIP6

10.1029/2022EF002972

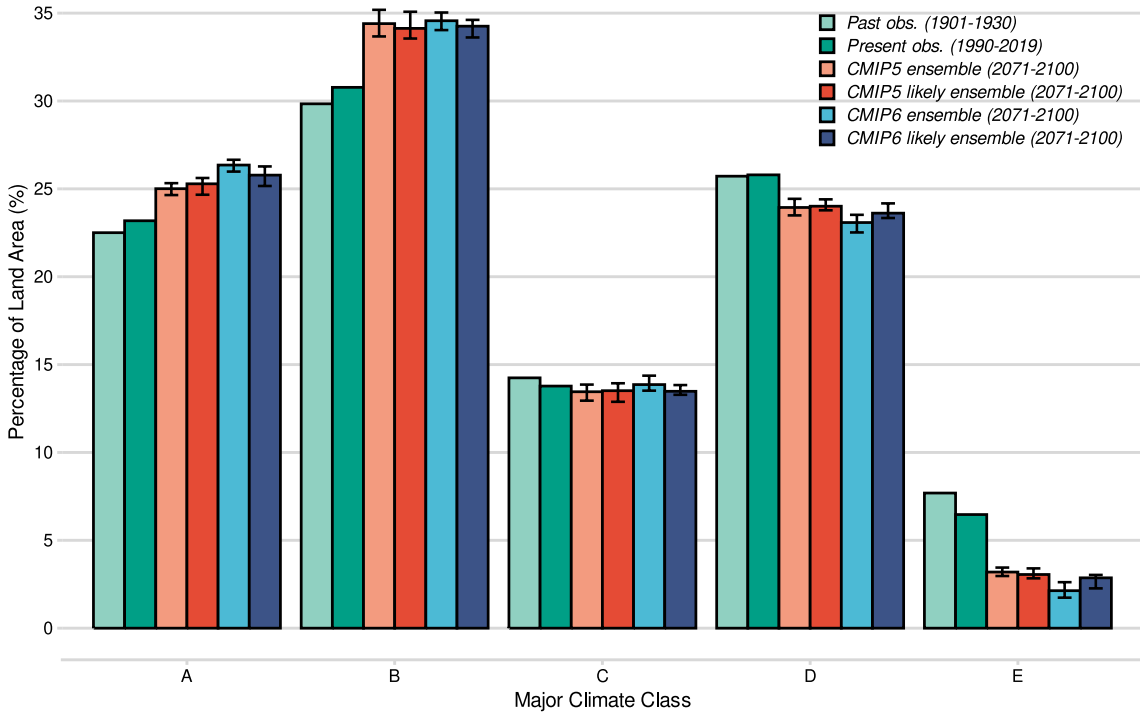

Figure 4. Percentage land area coverages of the major climate zones for past, present, and future periods. Error bars represent the 95% confidence interval for model ensemble projections.

ensemble (Hausfather et al., 2022). Although the levels of warming differ distinctively across the ensembles, colder high latitude climate zones are projected to experience more severe warming based on all ensemble projections, causing stronger shifts in the climate zones toward the poles.

3.4. Distribution of Climate Zones

The percentage of global land area covered by each major Köppen-Geiger climate zone is shown in Figure 4. In the past (1901–1930), the zone of tropical climate (A) covered 22.51% of the land area, expanding to cover 23.18% in the present (1990–2019). This climate zone is projected to further expand to 25.01% [95% confidence interval: 24.67–25.32] in the future (2071–2100) CMIP5 ensemble and to 26.35% [25.98–26.66] in the CMIP6 ensemble projections. The percentages based on the likely ensemble projections converge toward each other: 25.29% [24.67–25.62] in the CMIP5 likely ensemble and 25.78% [25.16–26.28] in the CMIP6 likely ensemble. There is a projected expansion of the arid climate zone (B) with similar levels based on all model ensembles. The percentage of land area based on CMIP5 ensemble is 34.40% [33.67–35.19], based on CMIP6 ensemble is 34.57% [34.03–35.04], based on CMIP5 likely ensemble is 34.13% [33.55–35.08] and based on CMIP6 likely ensemble is 34.26% [33.62–34.62] compared to present (30.78%) and past (29.84%) percentages land areas.

There is no apparent trend for coverage of the temperate climate zone (C), remaining near the current percentage of 13.78%. There is a projected contraction in the cold/continental climate zone (D), from 25.72% in past observations and 25.80% for the present-day, to 23.94% [23.49–24.43] and 23.08% [22.52–23.52] based on CMIP5 and CMIP6 ensemble projections, and to 24.01% [23.78–24.40] and 23.62% [23.34–24.17] based on likely ensembles of CMIP5 and CMIP6, respectively. The most extreme change is projected to occur in the polar climate zone (E). According to observations between 1901 and 1930, it covered 7.69% of the land area and has already shrunk to 6.47% in the present-day climate. It is projected to shrink drastically according to both CMIP5 (3.19% [2.97–3.45]) and CMIP6 (2.13% [1.74–2.62]) projections. Projections for the percentage land area in the likely ensembles of CMIP5 and CMIP6 converge somewhat, with CMIP6 likely ensemble projecting a greater reduction: 2.86% [2.27–3.03] versus 3.05% [2.84–3.40] based on the CMIP5 likely ensemble.

The observed and projected changes in areal coverage percentages of all 30 Köppen-Geiger climate classes are shown in Figure 5 (The exact area coverages of each climate class for past, present, and future are given in Figure

23284277, 2023, 4, Downloaded from https://agupubs.onlinelibrary.wiley.com/doi/10.1029/2022EF002972 by Orta Dogu Teknik Universitesi, Wiley Online Library on [20/10/2023]. See the Terms and Conditions (https://onlinelibrary.wiley.com/terms-and-conditions) on Wiley Online Library for rules of use; OA articles are governed by the applicable Creative Commons License

23284277, 2023, 4, Downloaded from https://agupubs.onlinelibrary.wiley.com/doi/10.1029/2022EF002972 by Ota Dogu Teknik Universitesi, Wiley Online Library on [20/10/2023]. See the Terms and Conditions (https://onlinelibrary.wiley.com/terms-and-conditions) on Wiley Online Library for rules of use; OA articles are governed by the applicable Creative Commons License

S15 in Supporting Information S1). Similar to previous studies (H. E. Beck et al., 2018; Hanf et al., 2012), there is a projected expansion in the tropical savannah zone (Aw): land area coverages for past (Figure 5a), present (Figure 5b), future CMIP5 ensemble (Figure 5c), future CMIP5 likely ensemble (Figure 5d), future CMIP6 ensemble (Figure 5e), and future CMIP6 likely ensemble (Figure 5f) are 12.73%, 13.56%, 16.19% [15.44–17.07], 16.62% [16.06–17.52], 17.68% [17.20–18.05], and 17.39% [16.38–17.92], respectively. The projected expansion in hot steppe and hot desert climate zones (BWh and BSh) are also in line with previous studies (Hanf et al., 2012): BWh coverages are 14.31%, 14.73%, 18.02% [17.48–18.70], 17.65% [17.12–18.32], 17.77% [17.32–18.07], and 17.23% [16.70–17.67] where BSh coverages are 6.03%, 6.91%, 8.29% [7.97–8.55], 8.37% [8.04–8.85], 8.70% [8.47–9.18], and 8.62% [8.38–9.06] respectively, for past, present, CMIP5 ensemble, CMIP5 likely ensemble, CMIP6 ensemble, and CMIP6 likely ensemble.

For the cold/continental climate zones (D), there is a notable trend in both CMIP5 and CMIP6 projections from cold summers (especially Dfc) toward hot summers (especially Dfa) in the mid-latitudes of Asia and North America, with the trend becoming more pronounced in CMIP6. Consistent with previous CMIP5 studies (Mahlstein et al., 2013), Dfc coverage shrinks while Dfa expands in time: Dfc coverages are 10.52%, 10.10%, 5.67% [4.83–6.29], 4.95% [4.31–5.63], 3.46% [2.64–4.02], and 4.70% [4.21–5.58], while Dfa coverages are 1.40%, 1.73%, 5.55% [4.48–7.08], 6.54% [5.57–7.97], 9.46% [8.64–10.37], and 6.93% [6.10–8.51] based on past observations, present observations, CMIP5 ensemble, CMIP5 likely ensemble, CMIP6 ensemble, and CMIP6 likely ensemble, respectively. Although the differences between the two generations are notable for the ensembles of the two CMIP generations (Figure 5g), they become marginal when the projections of the likely ensembles are compared (Figure 5h).

3.5. Global and Continental Climate Zone Changes

Global past, present, and future Köppen-Geiger maps (Figures 1 and 2) indicate that some continents are projected to experience greater changes in their present-state climate zones than others. Since the beginning of the 20th century, the Earth has already experienced 14.77% of its land area changing its climate classification, with the most extensive changes observed over North America, Europe, and Oceania (Figure S16 in Supporting Information S1). Furthermore, the CMIP5 ensemble simulates a world where 37.94% [35.27–41.53] of the climate zones will change by the end of the 21st century compared to present-day climate zones (Figure 6a), while the CMIP5 likely ensemble projects 39.66% [38.36–43.46] of global change (Figure 6b). These are lower than the 46.3% level obtained by Feng et al. (2014) but higher than the 20% level obtained by Mahlstein et al. (2013). The lower level found in the latter study is because Mahlstein et al. (2013) used linearly detrended time series to eliminate short-term climate variability, whereas we retain this information so as not to risk unintentional elimination of real signal. The change is even more pronounced in CMIP6, as the global percentage area of future classification change is projected to be 48.09% [45.36–50.97] based on the CMIP6 ensemble (Figure 6c), and 41.92% [40.29–45.62] based on the CMIP6 likely ensemble (Figure 6d). In all four CMIP5 and CMIP6 ensembles, Asia, Europe, and North America have higher percentage of areas projected to change, while Africa, Oceania, and South America have values below the global mean (Figure 6).

The two most sensitive continents to climate zone changes are projected to be Europe, then North America, in all CMIP5 and CMIP6 projections. 71.36% [65.55–79.34], 77.06% [69.75–81.41], 88.62% [84.54–91.20] and 80.93% [76.29–86.21] of Europe's land area is projected to be in a different climate zone than present-day based on the CMIP5 ensemble (Figure 6a), CMIP5 likely ensemble (Figure 6b), CMIP6 ensemble (Figure 6c), and CMIP6 likely ensemble (Figure 6d), respectively. Likewise, 51.19% [45.20–56.24], 55.02% [51.30–59.90], 65.79% [61.85–69.72], and 57.47% [54.82–63.17] of North America is projected to be in a different climate zone based on same four ensembles.

3.6. Rate of Climate Zone Change

Figure 7a shows the rate of areal climate zone change (10^6 km^2/year), in the observations and model ensembles. The rate of change in the GCMs for the historical period is substantially lower than that of observations until the 1990s, probably because internal climate variability induces most of the climate zone shifts until this time, and our frequency-based ensemble approach quells internal variability to some degree. However, the rate of change accelerates after the 1990s in both GCM generations for all the ensemble combinations, and in observations,

10.1029/2022EF002972

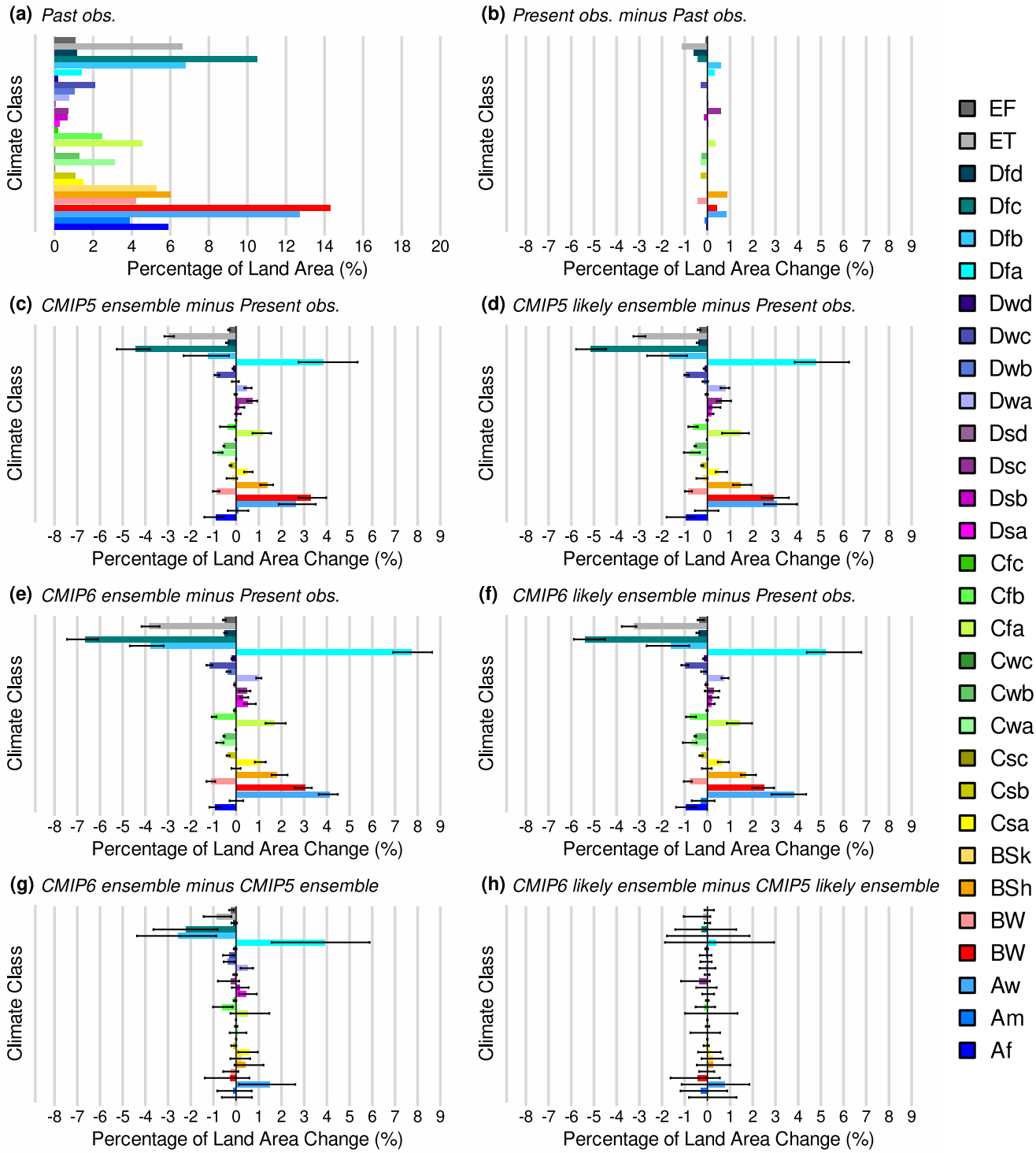

Figure 5. Percentage of the global land area for all 30 Köppen-Geiger climate classes based on (a) past (1901–1930) observations, (b) the difference between present-day (1990–2019) and past observations, (c) the difference between future (2071–2100) Coupled Model Intercomparison Project Phase 5 (CMIP5) ensemble and present-day observations, (d) the difference between future CMIP5 likely ensemble and present-day observations, (e) the difference between future Coupled Model Intercomparison Project Phase 6 (CMIP6) ensemble and present-day observations, (f) the difference between future CMIP6 likely ensemble and present-day observations, (g) the difference between future CMIP6 and CMIP5 ensembles, (h) the difference between future CMIP6 and CMIP5 likely ensembles. The land area change percentages represent the absolute change in the areas of climate classes (e.g., a −3% projected decrease in a climate class that covers 7% of the present-day land area means 4% projected future land area coverage). Error bars represent the 95% confidence interval for model ensemble projections.

23284277, 2023, 4, Downloaded from https://agupubs.onlinelibrary.wiley.com/doi/10.1029/2022EF002972 by Orta Dogu Teknik Universitesi, Wiley Online Library on [20/10/2023]. See the Terms and Conditions (https://onlinelibrary.wiley.com/terms-and-conditions) on Wiley Online Library for rules of use; OA articles are governed by the applicable Creative Commons License

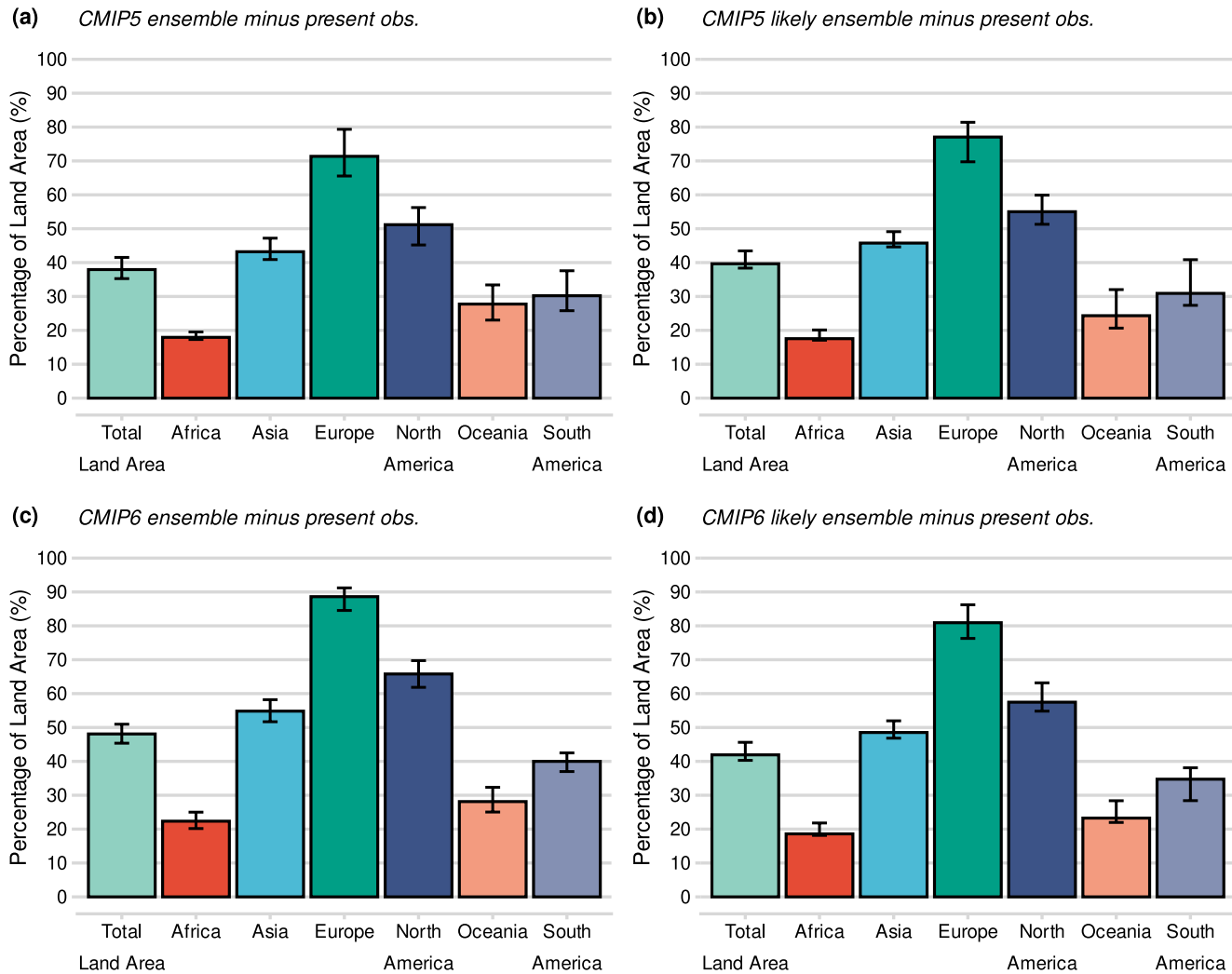

Figure 6. Percentage of land area globally and by continent that is projected to be in a different climate zone by 2071–2100 compared to the present-day observations; (a) based on the Coupled Model Intercomparison Project Phase 5 (CMIP5) RCP8.5 ensemble, (b) based on the CMIP5 RCP8.5 likely ensemble, (c) based on the Coupled Model Intercomparison Project Phase 6 (CMIP6) SSP5-8.5 ensemble, (d) based on the CMIP6 SSP5-8.5 likely ensemble. Error bars represent the 95% confidence interval for model ensemble projections.

when the climate warming signal starts to predominate over internal variability. Greater acceleration of change is projected in the CMIP6 ensemble with higher change rates than in the CMIP5 ensemble throughout the 21st century. The ECS constrained CMIP6 likely ensemble still projects a higher rate of climate zone change (reaching 10^6 km^2/year by the end of the century relative to the 2041–2070 climatology) than the corresponding CMIP5 likely ensemble, although the difference between the two generations is smaller than that of the 25-member ensembles.

The smaller difference between the likely ensembles of the two generations signals that the steeper °C/year warming rates might be the culprit of the greater acceleration of climate zone change observed in the CMIP6 ensemble. To estimate whether the difference emerges due to different global mean land warming rates or spatial pattern differences between the two model generations, we examine the total land area changing its climate zone at different global mean land warming levels relative to the 1901–1930 observations (Figure 7b). Although the changing land area as a function of global land warming is also slightly greater for the CMIP6 ensemble than the CMIP5, the results suggest that the greater change rates observed in the CMIP6 are dominated mainly by the models' stronger warming rates rather than the spatial pattern differences between the two model generations. For a comparison of the change rates as a function of global land warming level for the individual and ensemble models with mutual rescaling, and calculation details please see Text S2, Figure S17 in Supporting Information S1 and

23284277, 2023, 4, Downloaded from https://agupubs.onlinelibrary.wiley.com/doi/10.1029/2022EF002972 by Orta Dogu Teknik Universitesi, Wiley Online Library on [20/10/2023]. See the Terms and Conditions (https://onlinelibrary.wiley.com/terms-and-conditions) on Wiley Online Library for rules of use; OA articles are governed by the applicable Creative Commons License

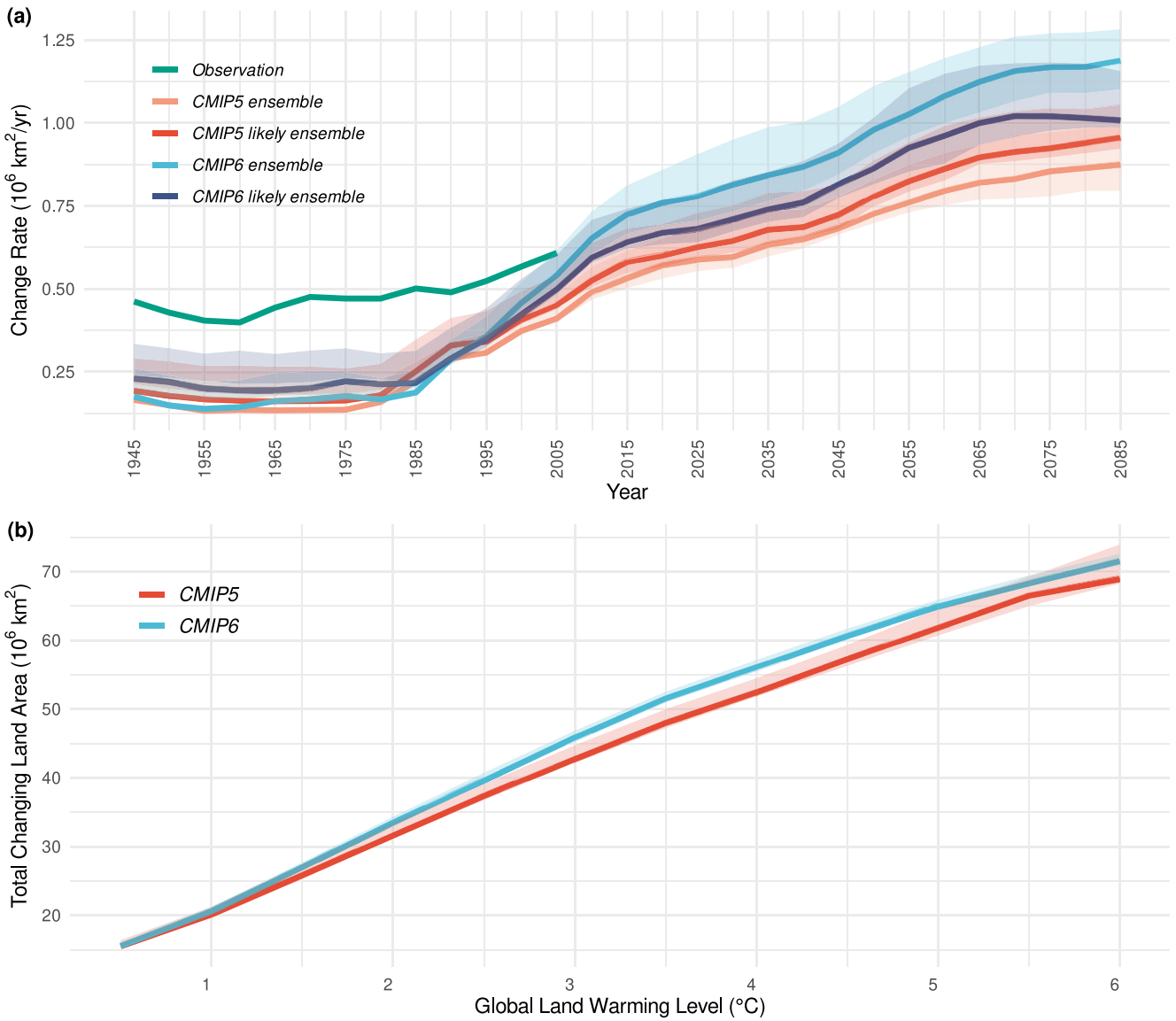

Figure 7. Rate of Climate Zone change and total land area undergoing climate zone change. (a) Rate of climate zone change as a function of time. (b) Total Land area changing its climate zone as a function of global mean land warming level relative to the baseline period observations for 1901–1930. Change rate as a function of time is calculated with the total area changing its climate zone between two consecutive 30-year time windows. Shaded bands represent the 95% confidence intervals for model ensemble projections.

Tables S1–S3 in Supporting Information S2. A previous study using CMIP5 simulations has also found that the pace of change in climate zones is dominated by the increasing global temperature rather than the changes in precipitation (Mahlstein et al., 2013).

We note that our CMIP5 and CMIP6 change rates do not lie within the 95% confidence intervals at the beginning of the calculation period in Figure 8a. That is probably because of the reason stated above: an individual model's internal variability is higher than the variability of our most frequent climate class-based approach for that period. Some models appear more than once for each bootstrap realization, and it limits the elimination of internal variability to some degree. Therefore, our CMIP5 and CMIP6 change rates remain lower than their confidence intervals for the earlier periods. However, after the 1990s, the climate warming signal becomes the dominant factor for the change rates, and our GCM-based change rates fall within their confidence intervals thereafter.

Figure 8 shows the loss rates of the five major climate zones (A–E). Loss rates of climate zones C, D, and E accelerated after 1980 in the observation period. Higher loss rates of these three climate zones are projected to

23284277, 2023, 4, Downloaded from https://agupubs.onlinelibrary.wiley.com/doi/10.1029/2022EF002972 by Orta Dogu Teknik Universitesi, Wiley Online Library on [20/10/2023]. See the Terms and Conditions (https://onlinelibrary.wiley.com/terms-and-conditions) on Wiley Online Library for rules of use; OA articles are governed by the applicable Creative Commons License

10.1029/2022EF002972

23284277, 2023, 4, Downloaded from https://agupubs.onlinelibrary.wiley.com/doi/10.1029/2022EF002972 by Orta Dogu Teknik Universitesi, Wiley Online Library on [20/10/2023]. See the Terms and Conditions (https://onlinelibrary.wiley.com/terms-and-conditions) on Wiley Online Library for rules of use; OA articles are governed by the applicable Creative Commons License

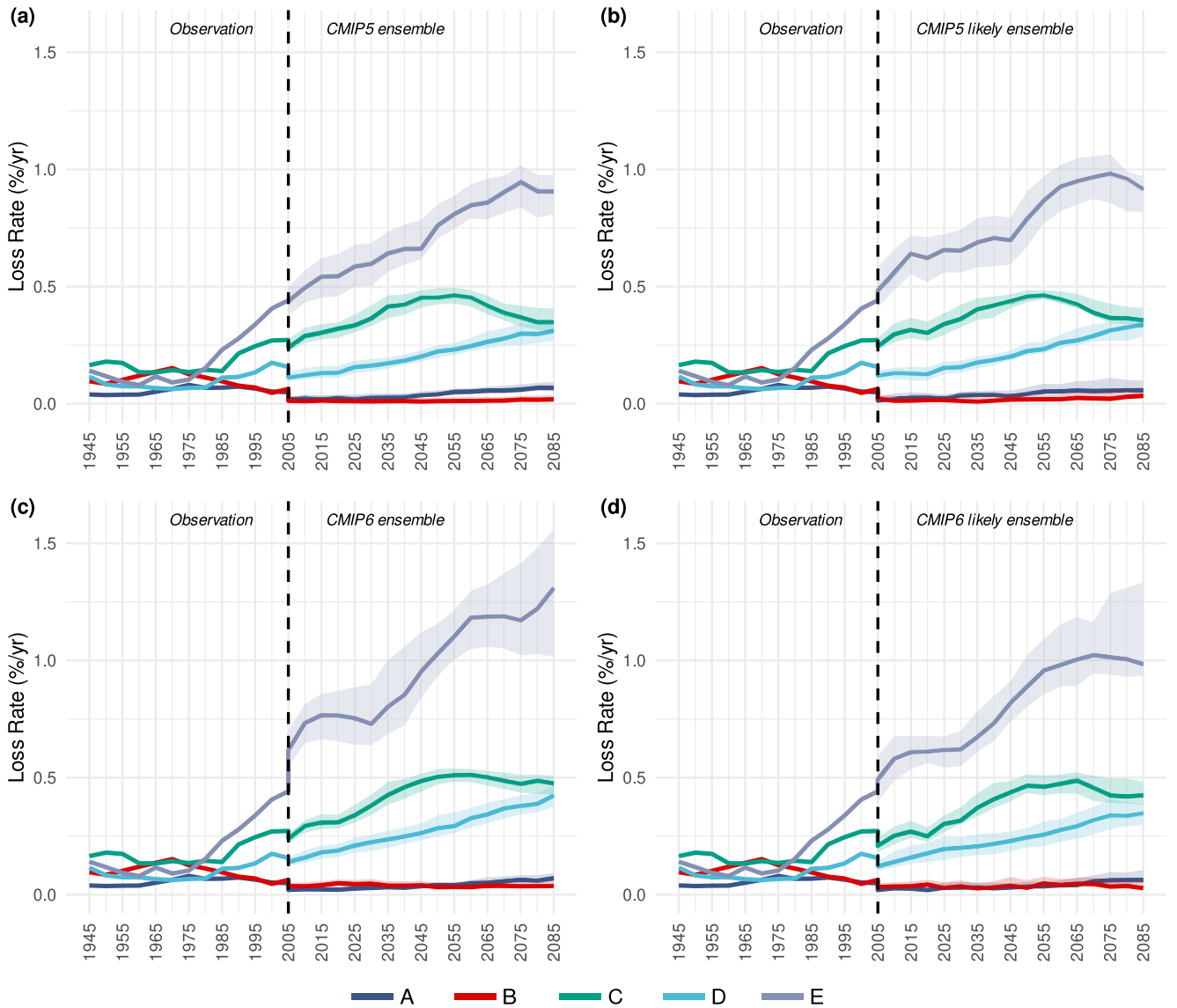

Figure 8. Loss rates of major climate zones based on observations and (a) the Coupled Model Intercomparison Project Phase 5 (CMIP5) ensemble, (b) the CMIP5 likely ensemble, (c) the Coupled Model Intercomparison Project Phase 6 (CMIP6) ensemble, (d) the CMIP6 likely ensemble. Shaded bands represent the 95% confidence interval for model ensemble projections.

remain higher in the future than the other two (A and B), with the polar (E) climate zone having the highest rate. Although both CMIP5 and CMIP6 simulations project an increasing trend in the loss rates of these three zones similarly, the magnitudes of the losses are more pronounced in CMIP6 compared to CMIP5 (Figures 8a and 8c). Yet, the gap between the two generations becomes smaller in the likely model subgroups (Figures 8b and 8d).

Figure 9 shows the total land areas of tropical (A) and arid (B) climate zones, which are projected to expand continuously throughout the 21st century for all ensembles of CMIP5 and CMIP6, despite the fluctuations that appeared in the 20th century. Importantly, having a constant area does not necessarily mean that the climate zone has not changed its geographical location (Mahlstein et al., 2013). There is no distinct trend in the area of the temperate (C) zone since it is projected to balance its lost areas by generally expanding toward the north, into the mid-latitudes of present-day cold (D) climate regions in the Northern Hemisphere, while it is harder to define a general trend over the Southern Hemisphere (Figures 1c, 1d, 2b, and 2c). Finally, there is a constant reduction in the projections of areal coverages of both cold (D) and polar (E) climate zones, with more explicit reductions in their areas projected in CMIP6. Once again, the gap between the two likely ensembles is smaller than that

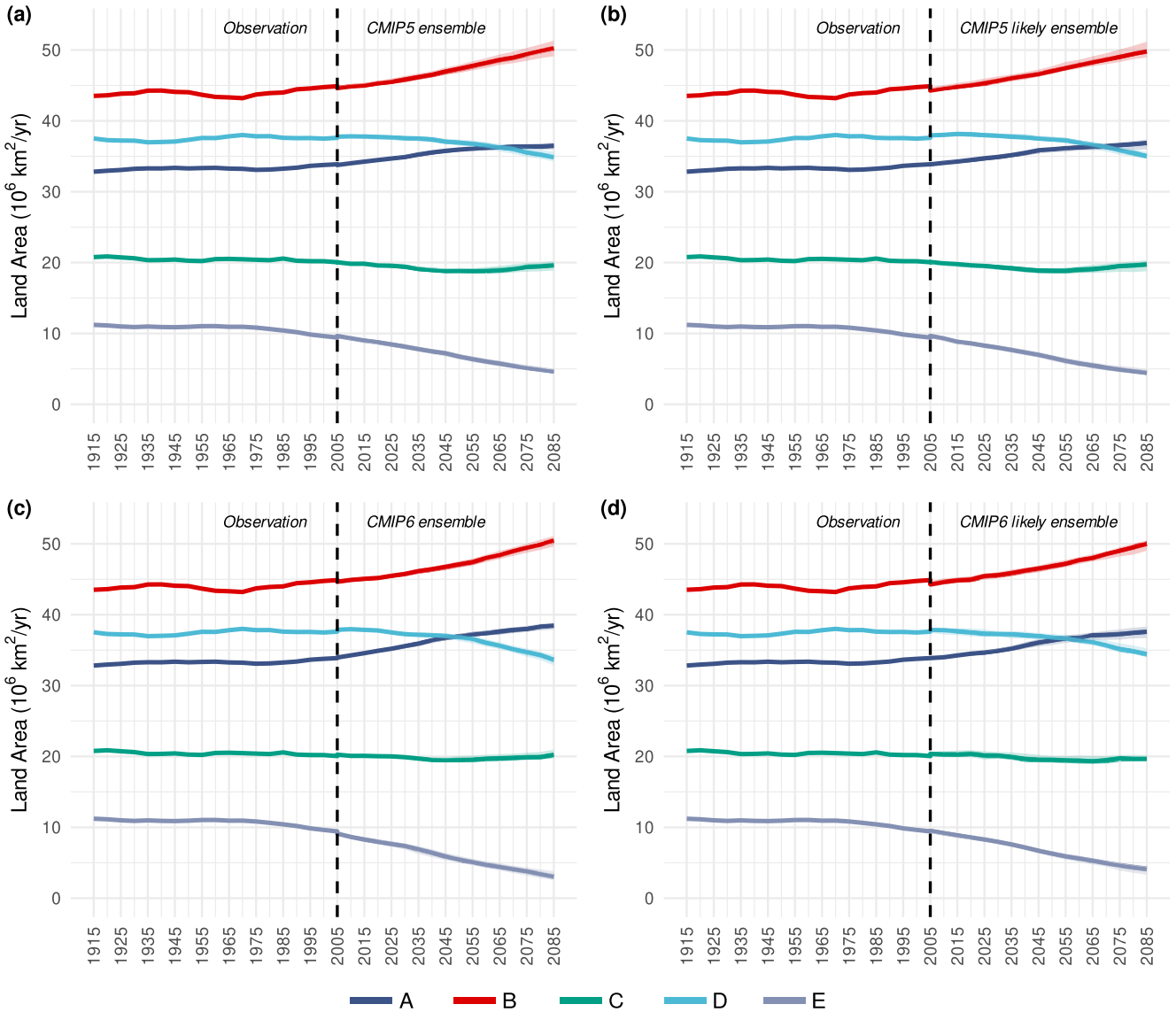

Figure 9. Total land areas occupied by the five major climate zones based on observations and (a) the Coupled Model Intercomparison Project Phase 5 (CMIP5) RCP8.5 ensemble, (b) the CMIP5 RCP8.5 likely ensemble, (c) the Coupled Model Intercomparison Project Phase 6 (CMIP6) SSP5-8.5 ensemble, (d) the CMIP6 SSP5-8.5 likely ensemble. Shaded bands represent the 95% confidence interval for model ensemble projections.

between the two 25-member ensembles, but the CMIP6 likely ensemble still projects greater reductions than CMIP5. The continuous dramatic reduction in the area coverage of the polar climate zone is because it cannot recover its lost areas by expanding into other locations.

4. Discussion and Conclusions

This study presents the observed and projected differences between the high-emission scenario GCMs in CMIP6 (SSP5-8.5) and the previous generation models of CMIP5 (RCP8.5) based on the Köppen-Geiger climate classification. Individual CMIP6 models, on average, have higher accuracy than CMIP5, where the ensemble-based CMIP6 estimate is only slightly better at representing the observed Köppen-Geiger climate classes for the reference period 1976–2005. However, similar bias patterns remain, which may result from some long-standing errors, such as the persistence of a double intertropical convergence zone (ITCZ) and Pacific cold tongue biases (Tian & Dong, 2020), despite the improvements in the new generation of CMIP6 models. Considering that there are uncertainties in the simulated climate zone distributions due to deficiencies in the physics of the models,

23284277, 2023, 4, Downloaded from https://agupubs.onlinelibrary.wiley.com/doi/10.1029/2022EF002972 by Orta Dogu Teknik Universitesi, Wiley Online Library on [20/10/2023]. See the Terms and Conditions (https://onlinelibrary.wiley.com/terms-and-conditions) on Wiley Online Library for rules of use; OA articles are governed by the applicable Creative Commons License

23284277, 2023, 4, Downloaded from https://agupubs.onlinelibrary.wiley.com/doi/10.1029/2022EF002972 by Orta Dogu Teknik Universitesi, Wiley Online Library on [20/10/2023]. See the Terms and Conditions (https://onlinelibrary.wiley.com/terms-and-conditions) on Wiley Online Library for rules of use; OA articles are governed by the applicable Creative Commons License

which particularly affect precipitation, further advancement in the parameterization of the physical processes of the models could lead to more accurate climate classifications in the future (Tapiador et al., 2019). Although CMIP6 models generally perform better during the historical period, their mean inter-model consistency in terms of assigning a common climate class to a grid for the future period (2071–2100) is slightly lower than that of CMIP5. On the other hand, such consistency among CMIP6 models is better in some regions in terms of temperature and precipitation climatology, for example, the Mediterranean (Bağçaci et al., 2021) and Sahel (Monerie et al., 2020).

We find that the subset of 11 CMIP6 models that lie within the likely ECS range as updated in the recent IPCC report (IPCC, 2021) projects greater warming over all 30 of the Köppen-Geiger climate zones by the end of the century than its CMIP5 counterpart (consisting of 16 models). However, the difference between the mean warming projections relative to the present-day observations over global land areas of the likely CMIP6 (4.45°C [4.09–4.80]) and CMIP5 (3.82°C [3.49–4.16]) ensembles are considerably smaller than that of the difference between projections from the larger CMIP6 (5.64°C [5.11–6.20]) and CMIP5 (4.29°C [3.93–4.66]) ensembles consisting of 25 models. The greater warming projections of the CMIP6 ensemble relative to the CMIP5 ensemble induce stronger shifts in their climate zone projections. On the other hand, the smaller warming difference between the likely model subsets of CMIP5 and CMIP6 causes these models to have more similar climate zone projections.

The increased warming trend observed in the CMIP6 projections does not alter the direction of changes in tropical, cold, and polar climates projected in CMIP5 but amplifies their magnitudes, whereas expansion of arid climate is projected nearly at the same level in both model generations. Moreover, the shift from cold summer to hot summer zones, such as Dfc to Dfa, in the mid-latitudes of the Northern Hemisphere, is projected to become more prominent in the CMIP6 projections versus CMIP5. Using the likely model ensembles does not change these conclusions, but projections of the percentage of land areas for the climate zones of CMIP5 and CMIP6 converge toward each other. As an important consequence of warming, this may result in greening in tundra areas and increased duration of the frost-free season in cold and polar climate zones.

By the end of the 21st century, climate zones over 37.94% [35.29–41.76] of the global land area are projected to change according to the CMIP5 projections, whereas the CMIP6 projections show a larger area of change: 47.95% [45.15–50.89]. The changing global land area projections of the two generations converge when the likely model subsets are used, but the CMIP6 likely ensemble still shows a larger change (41.92% [40.29–45.62]) than the CMIP5 likely ensemble (39.66% [38.36–43.46]). Also, Europe, North America, and Asia are projected to experience greater changes in their present-day climate zones than the global average in all four of the ensembles by the end of the century. Europe is projected to have the greatest change from the current climate, with 65%–91% of its land area projected to be in a different climate zone by the end of the century. Especially, the expansion of the temperate climate zone (C) into the present-day regions of cold (D) climate in Europe is projected to become salient by the end of the 21st century. However, a possible reason for relatively smaller projected changes in some continents might be the nature of the Köppen-Geiger climate classification. Since it is threshold-based, further increases (reductions) in the climatic conditions of a region already above (below) a threshold will not change its climate class even though the climate regime of the region is adversely affected, such as further temperature increases in the tropical climates of Africa (Mahlstein et al., 2013). Therefore, redefinition of climate classes might be necessary to account for the expected changes in the future climate.

The rate of climate zone change is projected to accelerate throughout the 21st century in both generations of climate model simulations, with higher rates projected in CMIP6. The change rates of likely ensembles converge toward each other, but the CMIP6 likely ensemble still has a greater change rate than that of the CMIP5 likely ensemble. Since there is a correlation between Köppen-Geiger climate zones and major biome types (Rohli et al., 2015), it implies that if the trajectory of the CMIP6 SSP5-8.5 scenario is to be followed, whether based on the likely ensemble or the 25-member ensemble, some vulnerable species with lower dispersal abilities in the regions with higher rates of change (Loarie et al., 2009; Sandel et al., 2011) might have less time to adapt to changes than previously projected by CMIP5 RCP8.5. Nevertheless, one should be cautious when relating the changes in the climate zones directly to actual biomes since there might be a delay in the vegetation changes, and other factors might affect the relationship between vegetation and climate zones (H. E. Beck et al., 2018), for instance, soil properties, pests, human intervention, and fertilization from increasing atmospheric CO_2 levels.

Although some models with high ECS could not simulate the observed warming trend well (Tokarska et al., 2020), we find that some of these models have high historical climate classification accuracies; hence they cannot be

completely discarded in an analysis based on climate classification. However, the converging projections of CMIP5 and CMIP6 likely ensembles against the diverging projections of the unconstrained model ensembles suggest that the difference in the climate zone projections between the two generations depends strongly on the ECS values of the models in the ensembles. We also find that the greater climate zone change rates simulated in CMIP6 are mainly dominated by the higher warming rates of these models. Since the plausibility of these high warming rate projections is a matter of debate, we recommend interpreting the likely model ensemble results as the more plausible future projections and the ensembles containing the models with high equilibrium climate sensitivities as the lower likelihood but potentially high-risk outcomes.

Data Availability Statement

CRU TS v4.04 monthly gridded temperature and precipitation data sets are available through https://crudata.uea.ac.uk/cru/data/hrg/. GPCC monthly gridded precipitation full data V.2020 can be downloaded via https://doi.org/10.5676/DWD_GPCC/FD_M_V2020_050. ERA5 reanalysis data are accessible through https://cds.climate.copernicus.eu/cdsapp#!/dataset/reanalysis-era5-single-levels-monthly-means. GHCN-CAMS temperature data can be downloaded via https://psl.noaa.gov/data/gridded/data.ghcncams.html. CMIP5 and CMIP6 global climate model data as described in Tables 1 and 2 are available through https://cds.climate.copernicus.eu/cdsapp#!/dataset/projections-cmip5-monthly-single-levels and https://cds.climate.copernicus.eu/cdsapp#!/dataset/projections-cmip6 or https://esgf-node.llnl.gov/projects/cmip5/ and https://esgf-node.llnl.gov/projects/cmip6/.

Acknowledgments
The open access publication fee for this research was provided by Center for Ocean-Land-Atmosphere Studies at George Mason University. We sincerely acknowledge the three reviewers and the editor whose valuable comments helped us improve the quality of the manuscript. We acknowledge the World Climate Research Programme (WCRP) and the climate modeling groups for coordinating, producing, and making available CMIP5 and CMIP6 data. We also thank the Earth System Grid Federation (ESGF) for archiving data and funding agencies that support CMIP5, CMIP6 and ESGF. We also gratefully acknowledge the observational temperature and precipitation data set developers. Ali Serkan Bayar thanks Eren Düzenli for providing feedback on the manuscript and the figures.

References

Andrews, T., Andrews, M. B., Bodas-Salcedo, A., Jones, G. S., Kuhlbrodt, T., Manners, J., et al. (2019). Forcings, feedbacks, and climate sensitivity in HadGEM3-GC3.1 and UKESM1. *Journal of Advances in Modeling Earth Systems*, *11*(12), 4377–4394. https://doi.org/10.1029/2019MS001866

Bağçaci, S. Ç., Yucel, I., Duzenli, E., & Yilmaz, M. T. (2021). Intercomparison of the expected change in the temperature and the precipitation retrieved from CMIP6 and CMIP5 climate projections: A mediterranean hot spot case, Turkey. *Atmospheric Research*, *256*, 105576. https://doi.org/10.1016/j.atmosres.2021.105576

Beck, C., Grieser, J., Kottek, M., Rubel, F., & Rudolf, B. (2005). Characterizing global climate change by means of Köppen climate classification. *Klimastatusbericht*, *51*, 139–149.

Beck, H. E., Zimmermann, N. E., McVicar, T. R., Vergopolan, N., Berg, A., & Wood, E. F. (2018). Present and future Köppen-Geiger climate classification maps at 1-km resolution. *Scientific Data*, *5*(1), 180214. https://doi.org/10.1038/sdata.2018.214

Belda, M., Holtanová, E., Halenka, T., Kalvová, J., & Hlávka, Z. (2015). Evaluation of CMIP5 present climate simulations using the Köppen-Trewartha climate classification. *Climate Research*, *64*(3), 201–212. https://doi.org/10.3354/cr01316

Bjordal, J., Storelvmo, T., Alterskjær, K., & Carlsen, T. (2020). Equilibrium climate sensitivity above 5°C plausible due to state-dependent cloud feedback. *Nature Geoscience*, *13*(11), 718–721. https://doi.org/10.1038/s41561-020-00649-1

Brunner, L., Pendergrass, A. G., Lehner, F., Merrifield, A. L., Lorenz, R., & Knutti, R. (2020). Reduced global warming from CMIP6 projections when weighting models by performance and independence. *Earth System Dynamics*, *11*(4), 995–1012. https://doi.org/10.5194/esd-11-995-2020

Chan, D., & Wu, Q. (2015). Significant anthropogenic-induced changes of climate classes since 1950. *Scientific Reports*, *5*(1), 13487. https://doi.org/10.1038/srep13487

Chen, D., & Chen, H. W. (2013). Using the Köppen classification to quantify climate variation and change: An example for 1901–2010. *Environmental Development*, *6*, 69–79. https://doi.org/10.1016/j.envdev.2013.03.007

Chen, I.-C., Hill, J. K., Ohlemüller, R., Roy, D. B., & Thomas, C. D. (2011). Rapid range shifts of species associated with high levels of climate warming. *Science*, *333*(6045), 1024–1026. https://doi.org/10.1126/science.1206432

Cui, D., Liang, S., & Wang, D. (2021). Observed and projected changes in global climate zones based on Köppen climate classification. *WIREs Climate Change*, *12*(3), e701. https://doi.org/10.1002/wcc.701

Dirmeyer, P. A., Fang, G., Wang, Z., Yadav, P., & Milton, A. (2014). Climate change and sectors of the surface water cycle in CMIP5 projections. *Hydrology and Earth System Sciences*, *18*(12), 5317–5329. https://doi.org/10.5194/hess-18-5317-2014

di Virgilio, G., Ji, F., Tam, E., Nishant, N., Evans, J. P., Thomas, C., et al. (2022). Selecting CMIP6 GCMs for CORDEX dynamical downscaling: Model performance, independence, and climate change signals. *Earth's Future*(4), e2021EF002625. https://doi.org/10.1029/2021EF002625

Efron, B. (1979). Bootstrap methods: Another look at the Jackknife. *Annals of Statistics*, *7*(1), 1–26. https://doi.org/10.1214/aos/1176344552

Eyring, V., Bony, S., Meehl, G. A., Senior, C. A., Stevens, B., Stouffer, R. J., & Taylor, K. E. (2016). Overview of the coupled model Intercomparison project phase 6 (CMIP6) experimental design and organization. *Geoscientific Model Development*, *9*(5), 1937–1958. https://doi.org/10.5194/gmd-9-1937-2016

Fan, Y., & van den Dool, H. (2008). A global monthly land surface air temperature analysis for 1948–present. *Journal of Geophysical Research*, *113*(D1), D01103. https://doi.org/10.1029/2007JD008470

Feng, S., Hu, Q., Huang, W., Ho, C. H., Li, R., & Tang, Z. (2014). Projected climate regime shift under future global warming from multi-model, multi-scenario CMIP5 simulations. *Global and Planetary Change*, *112*, 41–52. https://doi.org/10.1016/j.gloplacha.2013.11.002

Flato, G., Marotzke, J., Abiodun, B., Braconnot, P., Chou, S. C., Collins, W., et al. (2013). Evaluation of climate models. In T. F. Stocker, D. Qin, G.-K. Plattner, M. M. B. Tignor, S. K. Allen, J. Boschung, et al. (Eds.), *Climate change 2013: The physical science basis. Contribution of working group I to the fifth assessment report of the intergovernmental panel on climate change* (pp. 741–866). Cambridge University Press.

Forster, P. M., Maycock, A. C., McKenna, C. M., & Smith, C. J. (2020). Latest climate models confirm need for urgent mitigation. *Nature Climate Change*, *10*(1), 7–10. https://doi.org/10.1038/s41558-019-0660-0

Gettelman, A., Hannay, C., Bacmeister, J. T., Neale, R. B., Pendergrass, A. G., Danabasoglu, G., et al. (2019). High climate sensitivity in the Community Earth System Model Version 2 (CESM2). *Geophysical Research Letters*, *46*(14), 8329–8337. https://doi.org/10.1029/2019GL083978

23284277, 2023, 4, Downloaded from https://agupubs.onlinelibrary.wiley.com/doi/10.1029/2022EF002972 by Orta Dogu Teknik Universitesi, Wiley Online Library on [20/10/2023]. See the Terms and Conditions (https://onlinelibrary.wiley.com/terms-and-conditions) on Wiley Online Library for rules of use; OA articles are governed by the applicable Creative Commons License

Gnanadesikan, A., & Stouffer, R. J. (2006). Diagnosing atmosphere-ocean general circulation model errors relevant to the terrestrial biosphere using the Köppen climate classification. *Geophysical Research Letters*, *33*(22), L22701. https://doi.org/10.1029/2006GL028098

Golaz, J. C., Caldwell, P. M., van Roekel, L. P., Petersen, M. R., Tang, Q., Wolfe, J. D., et al. (2019). The DOE E3SM coupled model version 1: Overview and evaluation at standard resolution. *Journal of Advances in Modeling Earth Systems*, *11*(7), 2089–2129. https://doi.org/10.1029/2018MS001603

Gregory, J. M., Ingram, W. J., Palmer, M. A., Jones, G. S., Stott, P. A., Thorpe, R. B., et al. (2004). A new method for diagnosing radiative forcing and climate sensitivity. *Geophysical Research Letters*, *31*(3), L03205. https://doi.org/10.1029/2003GL018747

Grose, M. R., Narsey, S., Delage, F. P., Dowdy, A. J., Bador, M., Boschat, G., et al. (2020). Insights from CMIP6 for Australia's future climate. *Earth's Future*, *8*(5), e2019EF001469. https://doi.org/10.1029/2019EF001469

Hanf, F., Körper, J., Spangehl, T., & Cubasch, U. (2012). Shifts of climate zones in multi-model climate change experiments using the Köppen climate classification. *Meteorologische Zeitschrift*, *21*(2), 111–123. https://doi.org/10.1127/0941-2948/2012/0344

Harris, I., Osborn, T. J., Jones, P., & Lister, D. (2020). Version 4 of the CRU TS monthly high-resolution gridded multivariate climate dataset. *Scientific Data*, *7*(1), 109. https://doi.org/10.1038/s41597-020-0453-3

Hausfather, Z., Marvel, K., Schmidt, G., Nielsen-Gammon, J., & Zelinka, M. (2022). Climate simulations: Recognize the 'hot model' problem. *Nature*, *605*(7908), 26–29. https://doi.org/10.1038/d41586-022-01192-2

Hersbach, H., Bell, B., Berrisford, P., Hirahara, S., Horányi, A., Muñoz-Sabater, J., et al. (2020). The ERA5 global reanalysis. *Quarterly Journal of the Royal Meteorological Society*, *146*(730), 1999–2049. https://doi.org/10.1002/qj.3803

IPCC. (2013). Climate change 2013: The physical science basis. In T. F. Stocker, D. Qin, G.-K. Plattner, M. M. B. Tignor, S. K. Allen, J. Boschung, et al. (Eds.), *Contribution of working group I to the fifth assessment report of the intergovernmental panel on climate change*. Cambridge University Press.

IPCC. (2021). Summary for policymakers. In V. Masson-Delmotte, P. Zhai, Y. Chen, L. Goldfarb, M. I. Gomis, S. Berger, et al. (Eds.), *Climate change 2021: The physical science basis. Contribution of working group I to the sixth assessment report of the intergovernmental panel on climate change* (pp. 3–32). Cambridge University Press.

Kate, M., & Céline, B. (2013). Identifying external influences on global precipitation. *Proceedings of the National Academy of Sciences*, *110*(48), 19301–19306. https://doi.org/10.1073/pnas.1314382110

King, M., Altdorff, D., Li, P., Galagedara, L., Holden, J., & Unc, A. (2018). Northward shift of the agricultural climate zone under 21st-century global climate change. *Scientific Reports*, *8*(1), 7904. https://doi.org/10.1038/s41598-018-26321-8

Köppen, W. (1936). Das geographische system der Klimate. In W. Köppen & R. Geiger (Eds.), *Handbuch der Klimatologie* (pp. 1–44). Gebruder Borntraeger.

Kottek, M., Grieser, J., Beck, C., Rudolf, B., & Rubel, F. (2006). World map of the Köppen-Geiger climate classification updated. *Meteorologische Zeitschrift*, *15*(3), 259–263. https://doi.org/10.1127/0941-2948/2006/0130

Leemans, R., & Eickhout, B. (2004). Another reason for concern: Regional and global impacts on ecosystems for different levels of climate change. *Global Environmental Change*, *14*(3), 219–228. https://doi.org/10.1016/j.gloenvcha.2004.04.009

Liang, Y., Gillett, N. P., & Monahan, A. H. (2020). Climate model projections of 21st century global warming constrained using the observed warming trend. *Geophysical Research Letters*, *47*(12), e2019GL086757. https://doi.org/10.1029/2019GL086757

Loarie, S. R., Duffy, P. B., Hamilton, H., Asner, G. P., Field, C. B., & Ackerly, D. D. (2009). The velocity of climate change. *Nature*, *462*(7276), 1052–1055. https://doi.org/10.1038/nature08649

Lun, Y., Liu, L., Cheng, L., Li, X., Li, H., & Xu, Z. (2021). Assessment of GCMs simulation performance for precipitation and temperature from CMIP5 to CMIP6 over the Tibetan Plateau. *International Journal of Climatology*, *41*(7), 3994–4018. https://doi.org/10.1002/joc.7055

Mahlstein, I., Daniel, J. S., & Solomon, S. (2013). Pace of shifts in climate regions increases with global temperature. *Nature Climate Change*, *3*(8), 739–743. https://doi.org/10.1038/nclimate1876

Maraun, D. (2016). Bias correcting climate change simulations - A critical review. *Current Climate Change Reports*, *2*(4), 211–220. https://doi.org/10.1007/s40641-016-0050-x

Mccain, C. M., & Colwell, R. K. (2011). Assessing the threat to montane biodiversity from discordant shifts in temperature and precipitation in a changing climate. *Ecology Letters*, *14*(12), 1236–1245. https://doi.org/10.1111/j.1461-0248.2011.01695.x

McLaughlin, J. F., Hellmann, J. J., Boggs, C. L., & Ehrlich, P. R. (2002). Climate change hastens population extinctions. *Proceedings of the National Academy of Sciences*, *99*(9), 6070–6074. https://doi.org/10.1073/pnas.052131199

Meehl, G. A., Senior, C. A., Eyring, V., Flato, G., Lamarque, J.-F., Stouffer, R. J., et al. (2020). Context for interpreting equilibrium climate sensitivity and transient climate response from the CMIP6 Earth system models. *Science Advances*, *6*(26), eaba1981. https://doi.org/10.1126/sciadv.aba1981

Mehran, A., AghaKouchak, A., & Phillips, T. J. (2014). Evaluation of CMIP5 continental precipitation simulations relative to satellite-based gauge-adjusted observations. *Journal of Geophysical Research: Atmospheres*, *119*(4), 1695–1707. https://doi.org/10.1002/2013JD021152

Mehrotra, R., & Sharma, A. (2015). Correcting for systematic biases in multiple raw GCM variables across a range of timescales. *Journal of Hydrology*, *520*, 214–223. https://doi.org/10.1016/j.jhydrol.2014.11.037

Monerie, P.-A., Wainwright, C. M., Sidibe, M., & Akinsanola, A. A. (2020). Model uncertainties in climate change impacts on Sahel precipitation in ensembles of CMIP5 and CMIP6 simulations. *Climate Dynamics*, *55*(5), 1385–1401. https://doi.org/10.1007/s00382-020-05332-0

Navarro, A., Merino, A., Sánchez, J. L., García-Ortega, E., Martín, R., & Tapiador, F. J. (2022). Towards better characterization of global warming impacts in the environment through climate classifications with improved global models. *International Journal of Climatology*, *42*(10), 5197–5217. https://doi.org/10.1002/joc.7527

Ortega, G., Arias, P. A., Villegas, J. C., Marquet, P. A., & Nobre, P. (2021). Present-day and future climate over central and South America according to CMIP5/CMIP6 models. *International Journal of Climatology*, *41*(15), 6713–6735. https://doi.org/10.1002/joc.7221

Papadimitriou, L. V., Koutroulis, A. G., Grillakis, M. G., & Tsanis, I. K. (2017). The effect of GCM biases on global runoff simulations of a land surface model. *Hydrology and Earth System Sciences*, *21*(9), 4379–4401. https://doi.org/10.5194/hess-21-4379-2017

Parmesan, C., Ryrholm, N., Stefanescu, C., Hill, J. K., Thomas, C. D., Descimon, H., et al. (1999). Poleward shifts in geographical ranges of butterfly species associated with regional warming. *Nature*, *399*(6736), 579–583. https://doi.org/10.1038/21181

Parmesan, C., & Yohe, G. (2003). A globally coherent fingerprint of climate change impacts across natural systems. *Nature*, *421*(6918), 37–42. https://doi.org/10.1038/nature01286

Peel, M. C., Finlayson, B. L., & McMahon, T. A. (2007). Updated world map of the Köppen-Geiger climate classification. *Hydrology and Earth System Sciences*, *11*(5), 1633–1644. https://doi.org/10.5194/hess-11-1633-2007

Pereira, H. M., Leadley, P. W., Proença, V., Alkemade, R., Scharlemann, J. P. W., Fernandez-Manjarrés, J. F., et al. (2010). Scenarios for global biodiversity in the 21st century. *Science*, *330*(6010), 1496–1501. https://doi.org/10.1126/science.1196624

23284277, 2023, 4, Downloaded from https://agupubs.onlinelibrary.wiley.com/doi/10.1029/2022EF002972 by Ota Dogu Teknik Universitesi, Wiley Online Library on [20/10/2023]. See the Terms and Conditions (https://onlinelibrary.wiley.com/terms-and-conditions) on Wiley Online Library for rules of use; OA articles are governed by the applicable Creative Commons License

Phillips, T., & Bonfils, C. (2015). Köppen bioclimatic evaluation of CMIP historical climate simulations. *Environmental Research Letters*, *10*(6), 064005. https://doi.org/10.1088/1748-9326/10/6/064005

Riahi, K., van Vuuren, D. P., Kriegler, E., Edmonds, J., O'Neill, B. C., Fujimori, S., et al. (2017). The Shared Socioeconomic Pathways and their energy, land use, and greenhouse gas emissions implications: An overview. *Global Environmental Change*, *42*, 153–168. https://doi.org/10.1016/j.gloenvcha.2016.05.009

Ribes, A., Qasmi, S., & Gillett, N. P. (2021). Making climate projections conditional on historical observations. *Science Advances*, *7*(4), eabc0671. https://doi.org/10.1126/sciadv.abc0671

Rohli, R. V., Joyner, T. A., Reynolds, S. J., & Ballinger, T. J. (2015). Overlap of global Köppen-Geiger climates, biomes, and soil orders. *Physical Geography*, *36*(2), 158–175. https://doi.org/10.1080/02723646.2015.1016384

Rugenstein, M., Bloch-Johnson, J., Gregory, J., Andrews, T., Mauritsen, T., Li, C., et al. (2020). Equilibrium climate sensitivity estimated by equilibrating climate models. *Geophysical Research Letters*, *47*(4), e2019GL083898. https://doi.org/10.1029/2019GL083898

Sandel, B., Arge, L., Dalsgaard, B., Davies, R. G., Gaston, K. J., Sutherland, W. J., & Svenning, J. C. (2011). The influence of late quaternary climate-change velocity on species endemism. *Science*, *334*(6056), 660–664. https://doi.org/10.1126/science.1210173

Schneider, U., Becker, A., Finger, P., Meyer-Christoffer, A., Ziese, M., & Rudolf, B. (2014). GPCC's new land surface precipitation climatology based on quality-controlled in situ data and its role in quantifying the global water cycle. *Theoretical and Applied Climatology*, *115*(1), 15–40. https://doi.org/10.1007/s00704-013-0860-x

Sherwood, S. C., Webb, M. J., Annan, J. D., Armour, K. C., Forster, P. M., Hargreaves, J. C., et al. (2020). An assessment of Earth's climate sensitivity using multiple lines of evidence. *Reviews of Geophysics*, *58*(4), e2019RG000678. https://doi.org/10.1029/2019RG000678

Swart, N. C., Cole, J. N. S., Kharin, V. V., Lazare, M., Scinocca, J. F., Gillett, N. P., et al. (2019). The Canadian Earth system model version 5 (CanESM5.0.3). *Geoscientific Model Development*, *12*(11), 4823–4873. https://doi.org/10.5194/gmd-12-4823-2019

Tapiador, F. J., Moreno, R., & Navarro, A. (2019). Consensus in climate classifications for present climate and global warming scenarios. *Atmospheric Research*, *216*, 26–36. https://doi.org/10.1016/j.atmosres.2018.09.017

Taylor, K. E., Stouffer, R. J., & Meehl, G. A. (2012). An overview of CMIP5 and the experiment design. *Bulletin of the American Meteorological Society*, *93*(4), 485–498. https://doi.org/10.1175/BAMS-D-11-00094.1

Thomas, C. D., & Lennon, J. J. (1999). Birds extend their ranges northwards. *Nature*, *399*(6733), 213. https://doi.org/10.1038/20335

Tian, B., & Dong, X. (2020). The double-ITCZ bias in CMIP3, CMIP5, and CMIP6 models based on annual mean precipitation. *Geophysical Research Letters*, *47*(8), e2020GL087232. https://doi.org/10.1029/2020GL087232

Tokarska, K. B., Stolpe, M. B., Sippel, S., Fischer, E. M., Smith, C. J., Lehner, F., & Knutti, R. (2020). Past warming trend constrains future warming in CMIP6 models. *Science Advances*, *6*(12), eaaz9549. https://doi.org/10.1126/sciadv.aaz9549

Trewartha, G. T., & Horn, L. H. (1980). *An introduction to climate* (5th ed.). McGraw-Hill.

van Vuuren, D. P., Edmonds, J., Kainuma, M., Riahi, K., Thomson, A., Hibbard, K., et al. (2011). The representative concentration pathways: An overview. *Climatic Change*, *109*(1), 5–31. https://doi.org/10.1007/s10584-011-0148-z

Voldoire, A., Saint-Martin, D., Sénési, S., Decharme, B., Alias, A., Chevallier, M., et al. (2019). Evaluation of CMIP6 DECK experiments with CNRM-CM6-1. *Journal of Advances in Modeling Earth Systems*, *11*(7), 2177–2213. https://doi.org/10.1029/2019MS001683

Williams, J. W., Jackson, S. T., & Kutzbach, J. E. (2007). Projected distributions of novel and disappearing climates by 2100 AD. *Proceedings of the National Academy of Sciences*, *104*(14), 5738–5742. https://doi.org/10.1073/pnas.0606292104

Yin, L., Fu, R., Shevliakova, E., & Dickinson, R. E. (2013). How well can CMIP5 simulate precipitation and its controlling processes over tropical South America? *Climate Dynamics*, *41*(11), 3127–3143. https://doi.org/10.1007/s00382-012-1582-y

Zelinka, M. D., Myers, T. A., McCoy, D. T., Po-Chedley, S., Caldwell, P. M., Ceppi, P., et al. (2020). Causes of higher climate sensitivity in CMIP6 models. *Geophysical Research Letters*, *47*(1), e2019GL085782. https://doi.org/10.1029/2019GL085782

Zhang, X., Zwiers, F. W., Hegerl, G. C., Lambert, F. H., Gillett, N. P., Solomon, S., et al. (2007). Detection of human influence on twentieth-century precipitation trends. *Nature*, *448*(7152), 461–465. https://doi.org/10.1038/nature06025

Zhu, J., Poulsen, C. J., & Otto-Bliesner, B. L. (2020). High climate sensitivity in CMIP6 model not supported by paleoclimate. *Nature Climate Change*, *10*(5), 378–379. https://doi.org/10.1038/s41558-020-0764-6

23284277, 2023, 4, Downloaded from https://agupubs.onlinelibrary.wiley.com/doi/10.1029/2022EF002972 by Ota Dogu Teknik Universitesi, Wiley Online Library on [20/10/2023]. See the Terms and Conditions (https://onlinelibrary.wiley.com/terms-and-conditions) on Wiley Online Library for rules of use; OA articles are governed by the applicable Creative Commons License